## Title

Towards engineering nanobioreactors: characterization of bacterial microcompartment stability, regulation, and protein encapsulation



## Author

Kim, Edward

## Publication Date

2013

Peer reviewed|Thesis/dissertation

**Towards engineering nanobioreactors: characterization of bacterial microcompartment stability, regulation, and protein encapsulation**

By

Edward Yunyong Kim

A dissertation submitted in partial satisfaction of the

requirements for the degree of

Doctor of Philosophy

in

Chemical and Biomolecular Engineering

in the

Graduate Division

of the

University of California, Berkeley

Committee in charge:

Professor Danielle Tullman-Ercek, Chair
Professor Douglas Clark
Professor Arash Komeili

# ABSTRACT

**Towards engineering nanobioreactors: characterization of bacterial microcompartment stability, regulation, and protein encapsulation**

by

Edward Yunyong Kim

Doctor of Philosophy in Chemical and Biomolecular Engineering

University of California, Berkeley

Professor Danielle Tullman-Ercek, Chair

Compartmentalization of biological processes is an optimization strategy found throughout the biological world. On the cellular level, organelles act as compartments that allow for spatial and temporal control of biochemical reactions, as well as provide controlled microenvironments for these reactions. Bacteria generally lack the traditional membrane-enclosed organelles associated with eukaryotes. However, recent studies found that many bacterial species utilize microcompartments (MCPs) to carry out metabolic processes.

Bacterial MCPs have been suggested as scaffolds for nanobioreactors, in which biochemical pathways are targeted to the lumen of MCPs. The advantages of such an encapsulated pathway are many, including enhanced kinetics, sequestration of toxic intermediates, and insulation of internalized pathways from side reactions. MCPs may also prove to be an attractive protein cage for drug delivery. However, several challenges remain to be overcome to successfully repurpose naturally occurring MCPs into biotechnological tools.

Here, we first demonstrate that the propanediol utilization (Pdu) MCP of *Salmonella enterica* has the structural stability required for use as a nanobioreactor or in drug delivery applications. Transmission electron microscopy shows that the Pdu MCP is remarkably stable over time and is able to retain its structural integrity for several weeks at 4°C. The Pdu MCP is also able to maintain its structural integrity at temperatures up to 60°C, although aggregation of MCPs is observed above 50°C. On the other hand, the Pdu MCP is sensitive to pH and high salt, and denatures outside the range of pH 6 to pH 10, and in 1 M NaCl and 1 M urea.

We then investigate regulation of Pdu MCP formation. We find that PocR is a transcriptional activator of the *pdu* operon, and heterologous expression of PocR results in MCP formation in the absence of the natural inducer 1,2-propanediol. Next, we report the first instance of heterologous expression of the Pdu shell proteins in *Escherichia coli* in which MCPs form without morphological aberrations when compared to MCPs from the native host *S. enterica*.

Finally, we investigate the rules that govern the encapsulation of proteins within the Pdu MCP—a critical component for many of the proposed applications. Due to the time consuming process of MCP purification and subsequent western blot for detecting protein encapsulation using current methods, we first develop a rapid flow cytometry assay for quantifying the relative amount of protein encapsulated within MCPs based on fluorescence. Using this assay, we then characterize various MCP-targeting signal sequence mutants for their ability to encapsulate proteins and identify mutants that encapsulate a greater amount of protein than the wild type signal sequence. We demonstrate that this assay is a powerful tool for reporting protein encapsulation.

The studies presented here show that the Pdu MCP is a promising scaffold for nanobioreactors and drug delivery systems.

# TABLE OF CONTENTS

# LIST OF FIGURES

# LIST OF TABLES

# LIST OF ABBREVIATIONS

| | |
|---|---|
| 1,2-PD | 1,2-propanediol |
| aTc | Anhydrotetracycline |
| Eut | Ethanolamine utilization |
| GFP | Green fluorescent protein |
| LB | Lysogeny broth |
| MCP | Microcompartment |
| NCE | No-carbon E (media) |
| Pdu | Propanediol utilization |
| $PduP^{1-18}$ | Amino acids 1 through 18 of protein PduP |
| SsrA | The SsrA degradation peptide |

# ACKNOWLEDGEMENTS

I have many people to thank for their help and support throughout my PhD journey. I would first like to thank the undergraduate researchers Yuria Anaga, Sarena Horava, Christopher Laurel, and Kirk Mallet, as well as the graduate student Chris Jakobson, who have all contributed work towards what is presented here.

I would also like to thank the post-doc and fellow graduate students, not only for their helpful discussions and ideas, but for making the Tullman-Ercek lab such an enjoyable place. As colleagues turned into friends, work became something I looked forward to.

I would especially like to thank to my wonderful advisor, Danielle Tullman-Ercek, who was there for me from the very beginning and taught me how to set up my very first PCR. She took the time to ensure that I matured not only as a student, but that I grow in all aspects—as a scientist, as a presenter, as a writer, as a critical thinker, and much more.

To my mom, dad, and sister, who collectively have no idea what I have been doing for the past five and a half years but are nonetheless 100% supportive with their love—Thank you.

# Chapter 1: INTRODUCTION

## 1.1 Compartmentalization in nature

In nature, biochemical reactions are often spatially organized for optimization. A hallmark example of this strategy can be seen in the organelles of eukaryotes. Synthetic biologists and bioengineers have sought to mimic this grouping of related biochemical reactions by creating nanoscale assemblies of enzymes, particularly for *in vivo* applications. The primary benefit is the enhancement of overall kinetics due to the high local concentration of substrate in the vicinity for each enzyme of a given pathway. This effect has been demonstrated using enzymes linked together by scaffold proteins[1]. For the production of mevalonate in *Escherichia coli*, a 77-fold increase in yield was achieved for the scaffolded pathway compared to expression of the unscaffolded pathway[2]. The same concept was applied for trans-resveratrol biosynthesis using DNA-based scaffolds, resulting in a 5-fold increase in yield. Furthermore, the kinetic enhancements from DNA scaffolding were abolished when the spacer between enzymes was increased from 2bp to 850bp, emphasizing the importance of enzyme proximity[3].

Compartmentalization is expected to retain the advantage of enhanced kinetics that scaffolding provides. A stochastic model that explores the consequence of enzyme compartmentalization predicts that a compartmentalized *R*-1,2-propanediol biosynthetic pathway leads to a decrease in $K_m$ and therefore higher overall catalytic efficiency ($k_{cat}/K_m$) compared to the non-compartmentalized pathway[4]. The improved efficiency is greatest for substrates with low diffusivity. For substrates with diffusivities typical for small molecules, up to a 20% decrease in $K_m$ was predicted. Grouping the pathway enzymes in porous compartments provide additional advantages over simpler scaffolds, including control over molecules entering and exiting the compartment, custom microenvironments, and sequestration of toxic intermediates.

Many architectures have been proposed for such compartments both *in vivo* and *in vitro[5]*, including viral capsids[6-11], lumazine synthase capsids[12, 13], polymer cages[14, 15], liposomes[16], and bacterial microcompartments (MCPs). Although all of these options offer the structural support required to encapsulate enzymes, only one of these structures, bacterial MCPs, naturally evolved to encapsulate proteins. The MCP structure is a porous protein shell, offering the potential to control permeability of the compartment. Moreover, the process of encapsulating proteins can be done using genetic techniques *in vivo* rather than encapsulation by chemical means *in vitro*. These attributes have made bacterial MCPs attractive candidates for engineering nanobioreactors for use *in vivo*.

The most well-studied bacterial MCP systems include the carboxysome, the propanediol utilization (Pdu) MCP, and the ethanolamine utilization (Eut) MCP, though more are thought to exist[17, 18]. The first of these to be discovered was the carboxysome, found in all cyanobacteria[19]. However, cyanobacteria have relatively slow growth rates and more stringent growth conditions compared to other bacterial model organisms, making carboxysomes a more

difficult system to study. On the other hand, the Pdu and Eut MCPs are found in enteric bacteria. Of these two, there has been much recent progress towards with the characterization of the Pdu MCP system. The work presented here focuses on the Pdu MCP from *S. enterica* serovar Typhimurium LT2.

## 1.2 MCP structure

Bacterial MCPs have polyhedral protein shells that structurally resemble virus capsids (Figure 1.1 a), though there is no evidence for evolutionary relationship between the two structures[20]. The MCP shell, roughly 100-150 nm in diameter, is a multimeric structure composed of thousands of copies of a few proteins (Figure 1.1 b). Several MCP shell protein crystal structures have been solved, revealing many conserved structural motifs[21-30]. The most common repeating unit is a homohexamer that forms the facets of the polyhedral MCP shell (Figure 1.1 c). In addition, each MCP system contains a homologous shell protein (CcmL, CsoS4a, PduN, and EutN) that forms homopentamers, thought to provide the five-fold axis of symmetry required to form the vertices of the polyhedral shell[27, 31, 32]. A list of Pdu MCP associated proteins is given in Table 1.1.

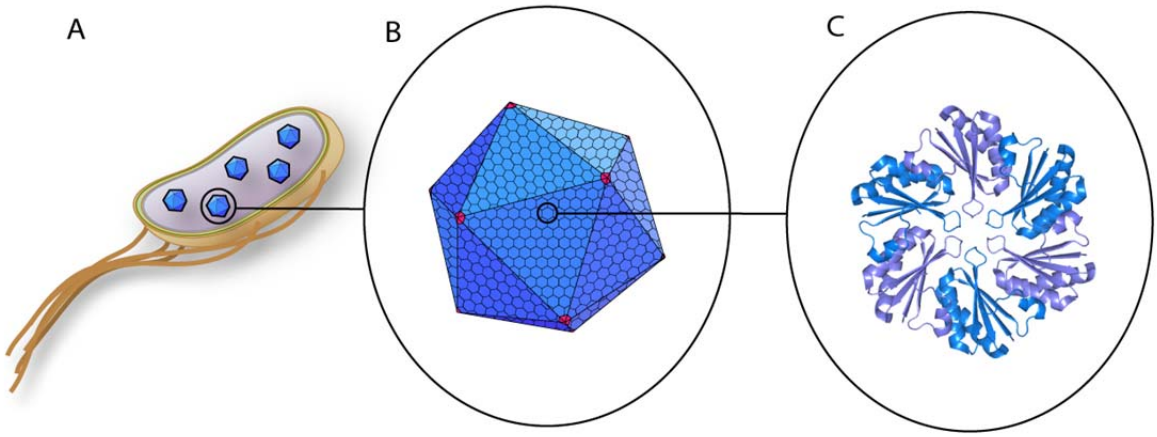


**Figure 1.1: Schematic of the Pdu MCP**
(a) *S. enterica*, when grown in the presence of 1,2-propanediol, expresses the Pdu MCP. (b) The Pdu MCP, approximately 100-150 nm in diameter, is composed of thousands of subunits, of which there are nine different types, that assemble to form a roughly polyhedral shell. (c) A close-up of the shell protein PduA shows that it assembles into a homohexamer in such a way that creates a central pore region thought to be responsible for the diffusion of small molecules into and out of the MCP.

**Table 1.1: List of Pdu MCP-associated proteins**
*Asterisks represent proteins with solved crystal structure

| MCP-localized proteins | Shell proteins |
|---|---|
| PduCDE | PduA* |
| PduGH | PduB |
| PduO | PduB' |
| PduP | PduJ |
| PduQ | PduK |
| PduS | PduM |
| PduV | PduN |
| | PduT* |
| | PduU* |

A central pore is created upon oligomerization of the shell proteins. Typically 4-16Å in diameter, this pore is thought to control the selective diffusion of metabolites into and out of the MCP[22, 28]. Supporting this theory, the pore regions of carboxysome hexamers are lined by positively charged amino acids which are thought to facilitate the diffusion of the negatively-charged substrates ribulose bisphosphate and bicarbonate into the MCP, and the product 3-phosphoglycerate out of the MCP. Meanwhile, the pore restricts the influx of neutrally-charged oxygen, a competing substrate for RuBisCO, and the outflux of $CO_2$, thereby creating a local microenvironment highly concentrated in $CO_2$. Similarly, in Pdu MCPs the inner surface of the PduA pore is mostly polar, and the exposed atoms present numerous sites for hydrogen bonding, providing a likely explanation for the permeability of the relatively polar substrate 1,2-propanediol and impermeability of the less polar intermediate propionaldehyde[22]. This selective diffusion also provides a means to sequester propionaldehyde, a reactive and toxic intermediate, within the MCP.

A few of the less-abundant shell constituent proteins have unique structural features, suggesting their specialized roles in MCPs. Two MCP shell proteins, the CsoS1D trimer of α-carboxysomes and the EutL trimer of the Eut MCP, have been crystallized in two different forms—one in which the pore is open and another in which the pore is closed[25, 30, 33]. A gated channel may be yet another way in which the MCP shell controls the diffusion of molecules into and out of the MCP. The PduT trimer has been suggested to contain a 4Fe-4S center[22, 23, 34]. This iron-sulfur cluster could be a means for the Pdu MCP shell to not only modulate small molecule transport, but electron flow as well. These capabilities may be useful for engineered pathways.

Even with our current limited understanding of MCPs, it is clear that MCPs have a complex and intricate design. To successfully implement MCPs as a biotechnological tool, we must first solve several technical challenges, such as gaining the ability to modify the MCP shell without disrupting MCP formation and engineering the MCP shell for increased stability.

## 1.3 Heterlogous shell protein expression and MCP assembly

As a step towards using MCPs as a biotechnological tool, there have been efforts to express MCPs in *E. coli* and to find the minimal set of genes required. The Pdu shell genes *pduA, -B, -B', -J, -K, -N, -T*, and *-U* from *Citrobacter freundii* were expressed in *E. coli* to produce empty

Pdu MCPs[35]. Two of these shell proteins were found to be non-essential for MCP formation, and Pdu MCPs were produced from expressing just *pduA, -B, -J, -K, -N*. In the native host *S. enterica*, however, it was reported that the protein PduM is also an essential shell protein for Pdu MCP formation, while PduA was found to be unnecessary[36, 37]. For the Eut system, empty Eut MCPs were produced in *E. coli* by the expression of *S. enterica* Eut shell genes *eutK, -L, -M, -N, S*[38]. Surprisingly, a minimal Eut MCP that was morphologically similar to wild type Eut MCPs was formed in *E. coli* by expression of EutS alone. Carboxysomes, naturally found in organisms more evolutionarily distant from *E. coli*, have also been produced in *E. coli* by the expression of nine genes from *Halothiobacillus neopolitanus[39]*. The ability to express a minimal MCP in *E. coli* shows promise towards using MCPs as modular tools in biotechnology.

There are also ongoing efforts to understand the assembly process of MCP shells. While fully assembled MCPs have been purified from expression host organisms (Figure 2b), there has been no successful *in vitro* MCP assembly from purified shell protein subunits. Although the structure for some of the shell proteins have been solved, the overall structural pattern of how these subunits come together, and in particular the stoichiometry among shell proteins, remains unclear. In the Pdu MCP, overexpression of individual shell proteins result in aberrant MCP formation, in some cases forming long thin fibers, rosettes, or large aggregates[34].

### 1.4 Enzyme Localization

Targeting heterologous proteins for encapsulation is a key step towards utilizing MCPs as customizable nanobioreactors. The mechanism for localization has been most well-characterized in the Pdu MCP system of *Salmonella enterica*. Bioinformatics has shown that MCP-associated homologs of the naturally-encapsulated proteins PduD, PduE, and PduP have N-terminal extensions compared to non-MCP-associated homologs. For two of these extensions, PduD and PduP, the fusion of the N-terminal 18 amino acids to heterologous proteins has been shown to be sufficient for localization to the lumen of the Pdu MCP[18, 40]. An additional signal sequence, the N-terminal 42 amino acids of PduV, was found to localize GFP to recombinant Pdu MCPs in *E. coli*[35]. However, fluorescence microscopy suggests that $PduV^{1-42}$-tagged GFP localizes to cup-like structures on the outer surface of the MCP. Similar work on the Eut genes from *S. enterica* have identified an N-terminal 19 amino acid peptide from EutC that was able to localize GFP to the lumen of recombinant Eut MCPs in *E. coli*[38]. For β-carboxysomes, a recent characterization of CcmN has shown that its C-terminus binds to the shell protein CcmK, suggesting its role as a localization signal sequence[41]. However, this putative signal sequence has not yet been shown to localize heterologous proteins into carboxysomes.

It should be noted that PduD, one of the aforementioned proteins shown experimentally to contain an N-terminal signal sequence, is a subunit of the three-subunit PduCDE holoenzyme. The large subunit of the holoenzyme, PduC, was not found to contain a signal sequence as marked by N-terminal extensions. Furthermore, PduC was only detected within MCPs in a Δ*pduCDE* knockout strain when coexpressed with PduD. Similar results were found for the small subunit PduE, suggesting that the signal sequence found on the N-terminus of PduD is sufficient to localize the entire PduCDE complex. Towards utilizing bacterial MCPs as synthetic organelles, this may allow for the encapsulation of multimeric enzymes without the burden of

tagging all subunits with a localization peptide, which may interfere with overall quaternary structure.

A general mechanism has been proposed for Pdu localization in which the signal sequence peptide binds to one of the MCP shell proteins. A pull-down assay has identified binding between PduP and shell protein PduA[42]. Truncation experiments with both binding partners revealed the regions responsible for binding to be the N-terminal 18 amino acids of PduP and the C-terminal 14 amino acids of PduA. An alanine scan for loss-of-localization mutants revealed three key residues in $PduP^{1-18}$ and three key residues in $PduA^{81-94}$. A structural model of the binding using RosettaDock reveals that these key residues align at the interface of the two alpha helices, further supporting that these residues are critical for binding.

## 1.5 Pdu MCP function

*S. enterica* express the Pdu MCP when grown in the presence of 1,2-propanediol (1,2-PD ) [43]. Thousands of copies of nine structural proteins form the outer shell which encapsulates the enzymes involved in the first two steps of 1,2-PD catabolism (Figure 1.2)[21, 23, 34-37, 44]. The substrate 1,2-PD is thought to diffuse through pores in the MCP shell where it is converted into propionaldehyde by diol dehydratase (PduCDE). Propionaldehyde, a highly reactive and toxic intermediate, is converted into propionyl-CoA by propionaldehyde dehydrogenase (PduP). The propionyl-CoA then exits the MCP where further catabolism steps occur in the cytoplasm of the cell. By encapsulating these first two steps of 1,2-PD catabolism in the lumen of the MCP, it is thought that the cell is shielded from the toxic intermediate propionaldehyde, which is quickly converted into a nontoxic intermediate before exiting the MCP [45].

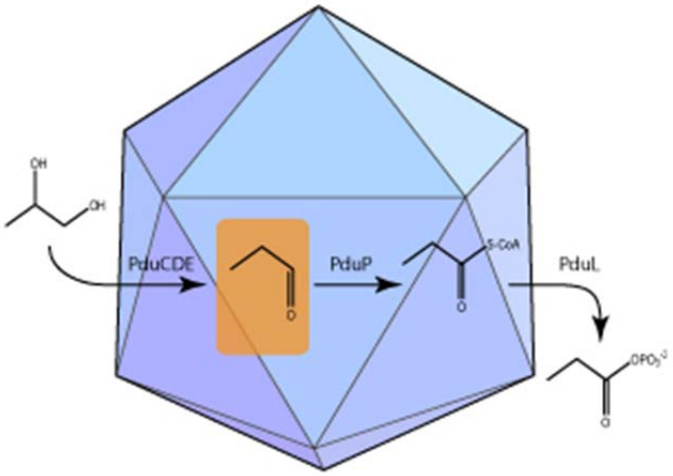


**Figure 1.2: Natural function of the Pdu MCP**
The first two steps of 1,2-PD catabolism occurs within the lumen of the Pdu MCP to sequester the toxic intermediate propionaldehyde.

## 1.6 Conclusions

The benefits of targeting synthetic pathways to MCPs are many. As observed in the natural function of the Pdu MCP, MCPs can sequester toxic intermediates in encapsulated synthetic pathways. Furthermore, compartmentalization is a method for insulating biochemical pathways from side reactions. While enzymes in engineered pathways can be modified to include an encapsulation signal sequence, competing enzymes cannot access encapsulated substrates. Finally, compartmentalization allows for custom microenvironments within MCPs. For example, oxidoreductases such as DsbA can be targeted to MCPs to create an oxidizing MCP microenvironment within a reducing cytosolic environment. The presence of an iron-sulfur cluster within one of the shell proteins, PduT, would facilitate the redox exchange in such a system[34].

As we push forward to expand our understanding of MCPs, we envision the development of many more novel applications.

# Chapter 2: STABILITY OF BACTERIAL MICROCOMPARTMENTS AND THE EFFECTS OF TIME, TEMPERATURE, AND PH.

## 2.1 Introduction

Microcompartments (MCPs) are a mechanism utilized by bacteria to organize and sequester enzymes and the biochemical pathways they catalyze[46, 47]. The Pdu MCP, involved in the catabolism of 1,2-propanediol (1,2-PD), is thought to have evolved for sequestration of the toxic intermediate propionaldehyde by encapsulation of the first two steps of the pathway [45]. The Pdu MCP shell is made up of thousands of copies of protein subunits, of which there are nine different types [21, 23, 34-37, 44]. The structures of several of these shell proteins have been solved, providing insight on how the subunits come together to form the polyhedral shell [21-30].

Recent studies show that MCPs are capable of encapsulating a variety of heterologous protein cargo [18, 38, 40, 42]. This feature lends itself to several applications. Recently, there has been much focus on utilizing MCPs to encapsulate synthetic enzymes to create nanobioreactors. The benefits of such a compartmentalized system are many, including control over which molecules enter and leave the MCP, kinetic enhancement from grouping enzymes, sequestration of toxic intermediates, and the ability to create custom microenvironments within the MCP [48]. Another application is to utilize MCPs as protein cages for drug delivery. Virus capsids, which share an analogous structural architecture, have already shown promise in this field [49-51]. In addition to offering many of the same advantages of a viral capsid delivery system, MCPs offer some unique advantages. The MCP shell is composed of multiple different shell proteins, ranging from high to very low copy number, some of which are non-essential [34]. This provides great versatility for making surface modifications to MCPs, such as coating the surface with cell-specific targeting peptides. Furthermore, cargo proteins can be encapsulated within MCPs *in vivo* using encapsulation signal peptides, eliminating the need for *in vitro* disassembly and reassembly of the shell and the additional purification steps required. Moreover, MCPs can easily be loaded with multiple different cargo proteins, a feat that normally requires additional chemistry in virus capsids.

One of the barriers currently limiting progress towards the practical application of bacterial MCPs is the lack of stability data. Studies on viruses show that protein capsids can range from being exceptionally stable, such as in the case of bacteriophage MS2 [52-54], to being transient and metastable, as with cowpea chlorotic mottle virus (CCMV) [55, 56]. Here, we seek to investigate the integrity of the Pdu MCP shell over time, at high temperatures, and at various pH. We find that MCPs are able to retain their morphological integrity for weeks at 4°C, and at temperatures up to 60°C. MCPs are, however, sensitive to pH and require conditions between pH 6 and pH 10. These results show that MCPs are robust and suitable for a wide variety of applications, and provide a starting point for engineering MCPs with higher stability.

## 2.2 Materials and Methods

### *2.2.1 Bacterial Strains, Media, and Growth Conditions*

The bacterial strain used in this study was *Salmonella enterica* serovar Typhimurium LT2. Cultures were grown in 2 ml of LB Miller medium overnight and subcultured 1:1000 into 400 ml of no-carbon-E (NCE) minimal medium[57] supplemented with 1 mM MgSO4, 50 μM ferric citrate, 0.5% succinate, 0.4% 1,2-propanediol, and antibiotic (17 μg/ml chloramphenicol) in a 2 L flask. Cells were grown at 37°C in an orbital shaker at 225 rpm. Upon reaching $OD_{600}$=0.4, 0.02% arabinose was added to induce the production of the reporter protein. After five additional hours of growth, 100 μl aliquots of cell culture were set aside for an *in vivo* MCP stability study, and the rest of the cells were harvested by centrifugation for Pdu MCP purification.

### 2.2.2 *Fluorescence microscopy*

Bacteria were viewed using a Nikon Ni-U upright microscope with a 100x , 1.45 n.a. plan apochromat objective. Images were captured using an Andor Clara-Lite digital camera. Fluorescence images were collected using a C-FL Endow GFP HYQ band pass filter.

### *2.2.3 Pdu MCP purification*

The following MCP purification protocol is adapted from a previously described method [36]. Harvested cell pellet was washed in 40 ml of buffer A (50 mM Tris-HCl, 500 mM KCl, 12,5 mM $MgCl_2$, 1.5% 1,2-PD, pH 8.0). Cells were resuspended in cell lysis buffer consisting of 10 ml buffer A, 15 ml B-PER II, 5 mM β-mercaptoethanol, 1 mM phenylmethanesulfonyl fluoride, 25 mg lysozyme, and 10 units of DNase I (NEB M0303S), and incubated at room temperature for 30 minutes. The cell lysate was clarified twice by centrifugation at 12,000 x g for 5 minutes at 4°C, then passed through a 0.45 μm filter to remove remaining cellular debris. MCPs were pelleted by centrifugation at 21,000 x g for 20 minutes at 4°C, washed with 4 ml of Buffer A and 6 ml of BPER-II, then pelleted again by centrifugation at 21,000 x g for 20 minutes at 4°C. The MCP pellet was resuspended in 300 μl of Buffer B (50 mM Tris-HCl, 50 mM KCl, 5 mM $MgCl_2$, 1% 1,2-PD, pH 8.0). Remaining debris was removed by three additional centrifugation steps at 12,000 x g for 1 minute at 4°C.

### *2.2.4 Electron microscopy*

10 μl of purified MCPs, at a concentration of 100 μg/ml, were placed on 400 mesh formvar coated copper grids with a carbon film for two minutes. The grids were washed three times with deionized water, then stained with 2% aqueous uranyl acetate for one minute. Samples were observed and photographed with a FEI Tecnai T12 transmission electron microscope.

### 2.2.5 *In-vivo temperature incubation*

100 µl samples of cell culture were centrifuged for 5 min at 5,000 g to pellet the cells. The supernatant was removed and the cells were resuspended in 400 µl phosphate buffered saline (PBS) with 50 µg/ml kanamycin to halt protein production. One sample was kept at 4°C, and the other at room temperature.

### 2.2.6 *Temperat*ure *incubation on purified MCPs*

50 µl of purified MCPs, at a concentration of 300 µg/ml, were incubated at the corresponding temperature for 15 minutes, then brought back to 4°C until they were processed for transmission electron microscopy (TEM).

### *2.2.7 pH, salinity, and denaturant conditions*

100 µl of purified MCPs, at a concentration of 300 µg/ml, were centrifuged for 30 minutes at 16,000 g to pellet the MCPs. The supernatant was removed and the MCPs were resuspended in 50 µl of the appropriate buffer. The buffers used to adjust pH are listed Table 2.1. For the high salinity and urea studies, the appropriate solute was dissolved in buffer B (50 mM Tris-HCl, 50mM KCl, 5 mM $MgCl_2$, 1% 1,2-PD, pH 8.0) [36].

**Table 2.1: Buffers for adjusting pH**

| Buffer | Buffer |
|---|---|
| pH 3 | 79.45 mM Citric acid, 41.1 mM sodium phosphate |
| pH 4 | 61.45 mM Citric acid, 77.1 mM sodium phosphate |
| pH 5 | 48.50 mM Citric acid, 103.0 mM sodium phosphate |
| pH 6 | 36.85 mM Citric acid, 126.3 mM sodium phosphate |
| pH 7 | 17.65 mM Citric acid, 164.7 mM sodium phosphate |
| pH 8 | 50 mM Tris |
| pH 9 | 50 mM Tris |
| pH 10 | 100 mM CAPS |
| pH 11 | 100 mM CAPS |

### *2.2.8 Dynamic light scattering*

100 µl of purified MCPs, at a concentration of 750 µg/ml, were placed in 8.5 mm disposable spectrophotometry cuvettes and analyzed on a Melvern Instruments Zen 3600. For temperature studies, the instrument was programmed to increase the temperature in increments of 5°C, equilibrate for five minutes, and record.

### *2.2.9 Thermofluor assay*

25 µl of purified MCPs, at a concentration of 300 µg/ml, were mixed with SYPRO Orange at a final concentration of 15X (SYPRO Orange is proprietary dye and the absolute concentration is not disclosed). The temperature was increased from 30°C to 75 °C by 0.2°C increments held for 12 seconds, and fluorescence was measured in a Bio-Rad CFX96 Touch Real-Time PCR Detection System.

## 2.3 Results

### *2.3.1 MCP integrity over time*

We first assessed the stability of the Pdu MCP *in vivo*. *S. enterica* expressing the reporter protein $PduP^{1-18}$-GFP, previously shown to encapsulate within the Pdu MCP[18, 42], was resuspended in PBS and 50 µg/ml of kanamycin to halt further protein production. Cells were imaged every 24 hours with a fluorescent microscope (Figure 2.1). The encapsulated reporter protein, seen as fluorescent puncta, remains present within cells for over one week whether held at 4°C or at room temperature. After nine days, MCPs held at room temperature began to lose overall fluorescence, and a high proportion of cells no longer contained fluorescent puncta. At this time it is unknown whether this is due to the disassembly of MCPs, disassociation of $PduP^{1-18}$-GFP from the Pdu MCP, or diffusion of intact MCPs out of the cytosol due to a compromised cellular membrane.

To assess the stability of the Pdu MCP *in vitro*, MCPs from the same strain were purified using a protocol previously described[36]. Purified MCPs were held at either 4°C or at room temperature, and transmission electron microscopy (TEM) was used to assess the integrity of the MCPs. TEM images show that after nine days, a portion of MCPs begin to form aggregates, but otherwise appear normal (Figure 2.2). After twenty-two days, MCPs held at room temperature show deterioration, although closer inspection shows areas containing MCPs that still retain their characteristic defined edges. On the other hand, MCPs held at 4°C appear normal after twenty-two days. Manual inspection of TEM images shows no significant change in apparent MCP diameter over time.

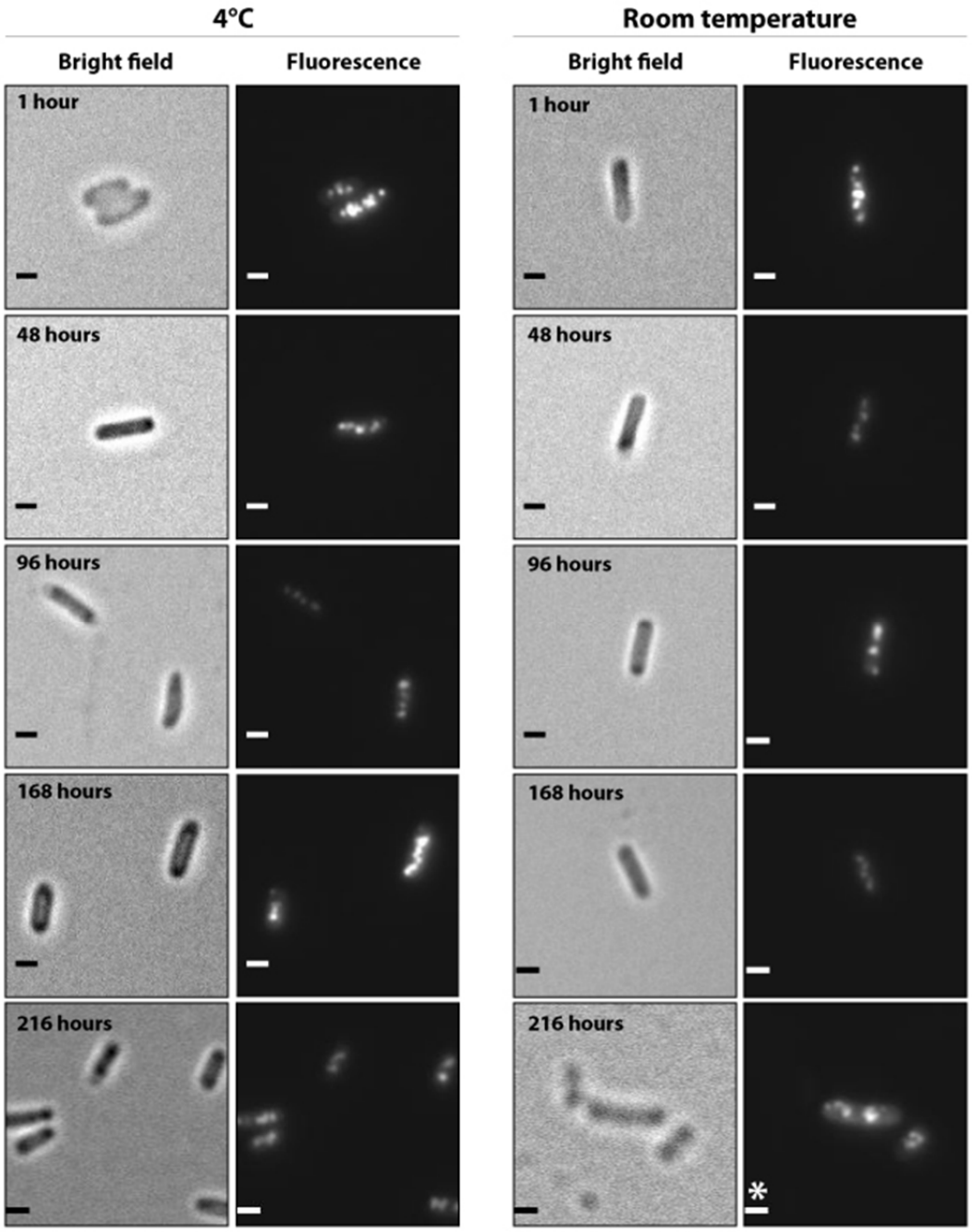


**Figure 2.1: Fluorescence microscopy time course of *S. enterica* expressing PduP$^{1-18}$-GFP**
*S. enterica* was resuspended in PBS with 50 μg/ml of kanamycin to halt further protein production. The encapsulated reporter protein appears as fluorescent puncta. The camera exposure times were 50 ms. For images marked by an asterisk (*) symbol, camera exposure times were 200 ms.

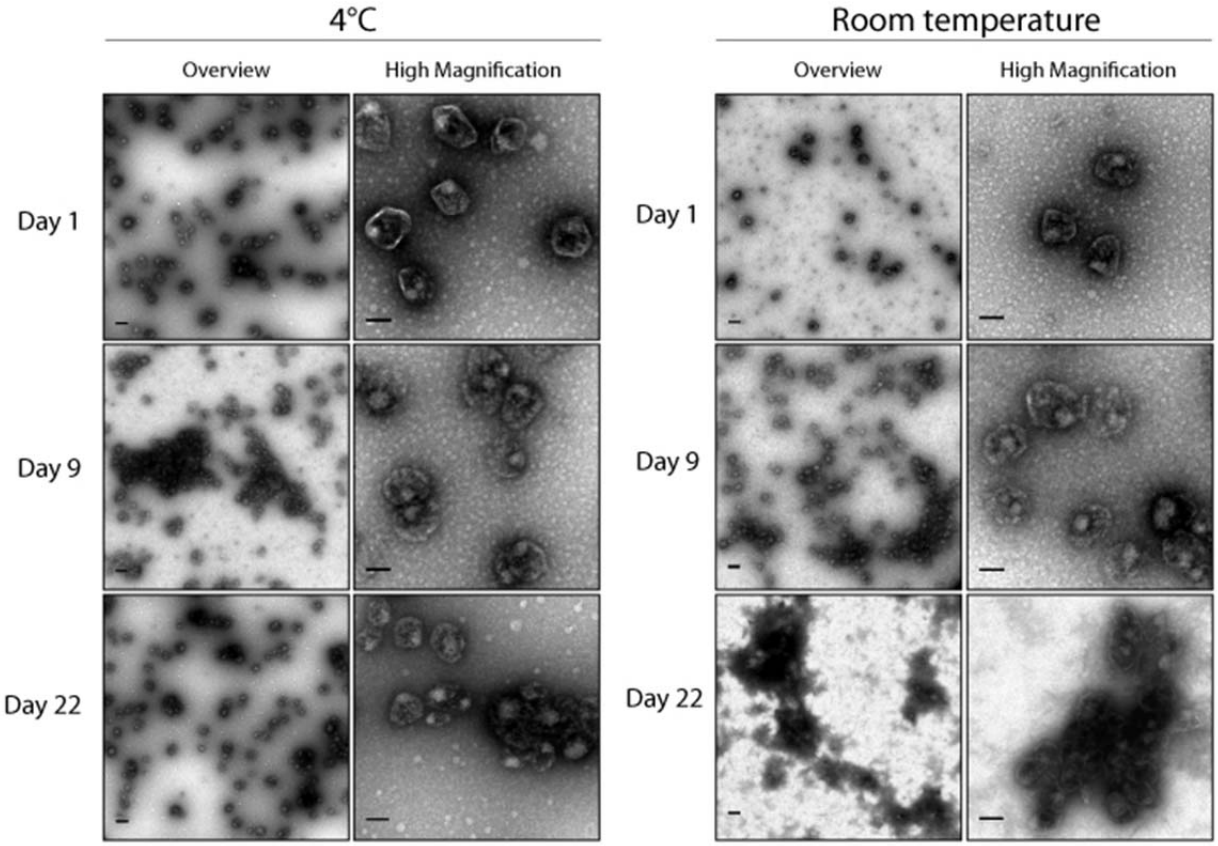


**Figure 2.2: TEM images of purified MCPs over time**
MCPs were held at either 4°C or at room temperature. Two representative images are shown for each time point. Scale bars represent 200 nm in overview images, and 100 nm in high magnification images.

### 2.3.2 *Heat-induced aggregation of MCPs*

Next, we probed the stability of the Pdu MCP held at elevated temperatures for 15 minutes. TEM images show that at temperatures up to 60°C, MCPs appear normal in size and retain their defined edges, although the amount of aggregation increases with increasing temperature (Figure 2.3). At 70°C and above, the majority of MCPs are found within large aggregates, although the outlines of the MCP bodies can be seen up to 90°C.

Dynamic light scattering (DLS) was used to complement TEM and further investigate the process of aggregation. A representative size distribution profile for MCPs without heat treatment shows agreement with estimated MCP diameters from TEM images (Figure 2.4 a). As temperature increases, aggregates begin to form, and the proportion of MCPs found in the aggregates increases with increasing temperature (Figure 2.4 b).

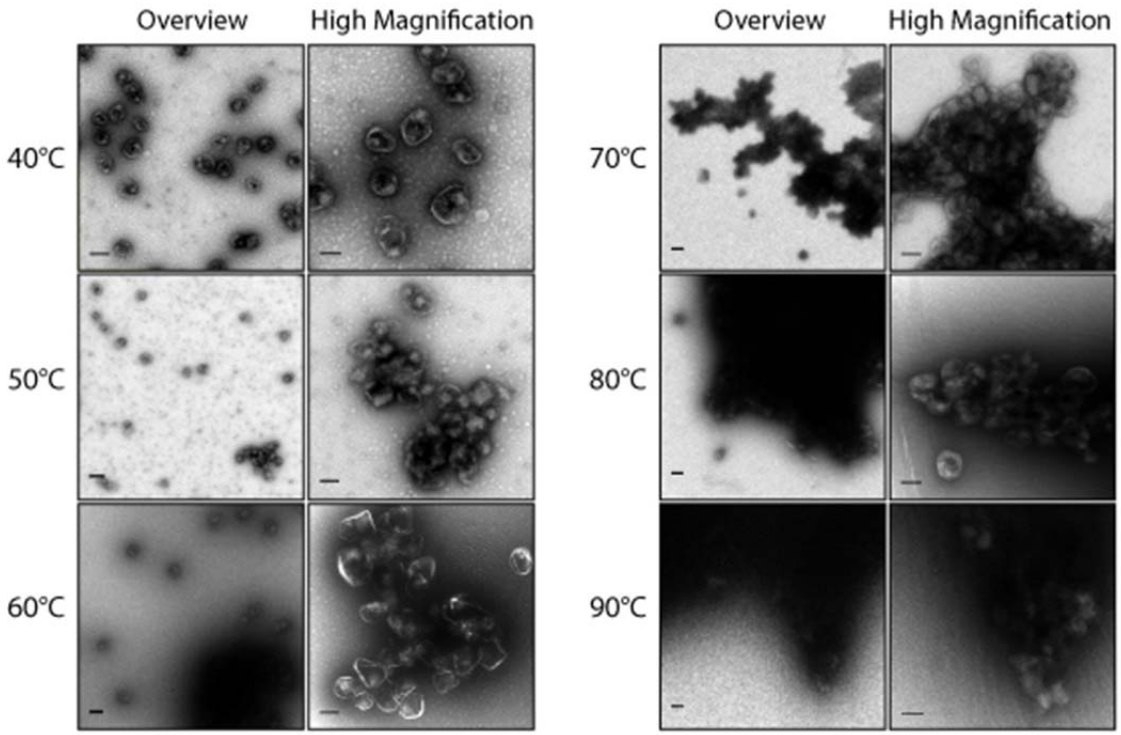


**Figure 2.3: TEM images of purified MCPs after incubation at elevated temperature**
Purified MCPs were incubated for fifteen minutes at elevated temperatures. Two representative images are shown for each time point. Scale bars represent 200 nm in overview images, and 100 nm in high magnification images.

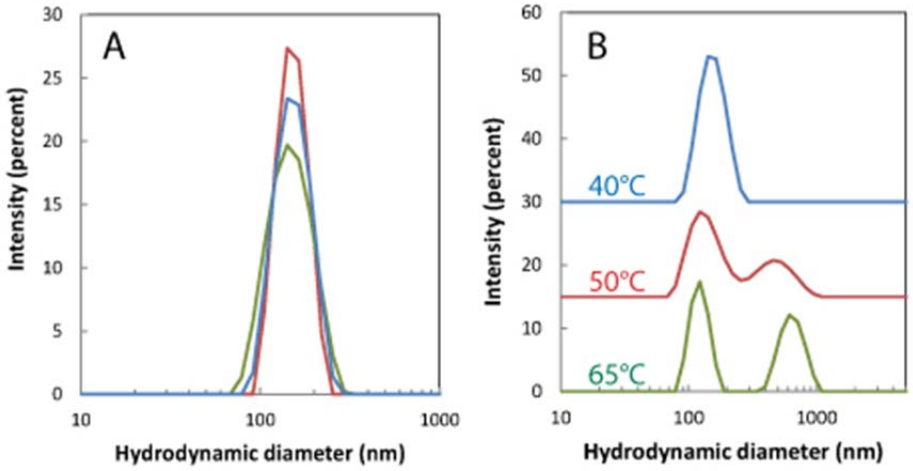


**Figure 2.4: Size distribution profile of MCPs using dynamic light scattering**
(a) Hydrodynamic diameter from three measurements of MCPs from *S. enterica* encapsulating PduP$^{1-18}$-GFP held at 4°C. (b) Representative DLS measurements of MCPs incubated at elevated temperatures.

We further investigate the stability of the Pdu MCP at elevated temperatures with a Thermofluor assay. In this assay, the dye SYPRO Orange fluoresces as it binds to hydrophobic patches of proteins as they undergo thermal unfolding [58-60]. The temperature increments and fluorescence readings can be performed in a qPCR thermocycler to generate a temperature profile for MCP thermal denaturation (Figure 2.5 a). The melting temperature is found at the inflection point of the temperature profile, which can be determined from the local maxima in the first derivative plot (Figure 2.5 b). We find that the Pdu MCP has a melting temperature of 52.1°C, which is approximately the temperature at which we begin to see aggregation of MCPs by TEM.

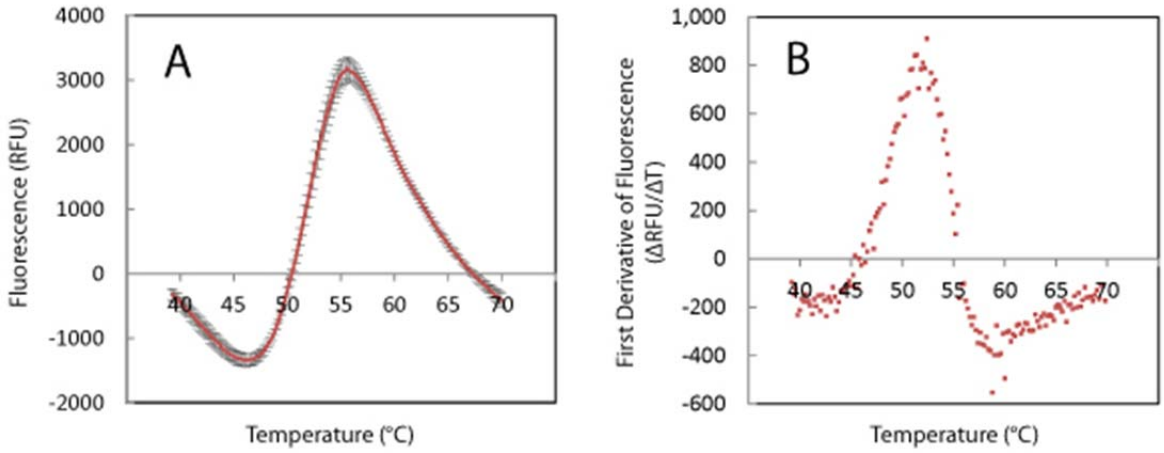


**Figure 2.5: MCP denaturation by a Thermofluor assay**
(a) MCP denaturation is measured by fluorescence of SYPRO Orange as temperature is raised.
(b) The first derivative plot of fluorescence is used to find the melting temperature.

### *2.3.3 MCP integrity at various pH, in high salt, and with urea*

Next, we probed the stability of MCPs in various buffer conditions. First, purified MCPs were resuspended in buffers of different pH. TEM images show that MCPs display normal morphology between the range of pH 6 and pH 10 (Figure 2.6). However, at pH 9 and pH 10, the majority of MCPs were found in large aggregates, and at pH 11 the MCP bodies show signs of denaturation, as the MCP bodies appear smaller than the typical 100 to 150 nm diameter previously reported [43, 44, 61] and with less defined edges. In acidic conditions, MCPs denature at pH 5 and below.

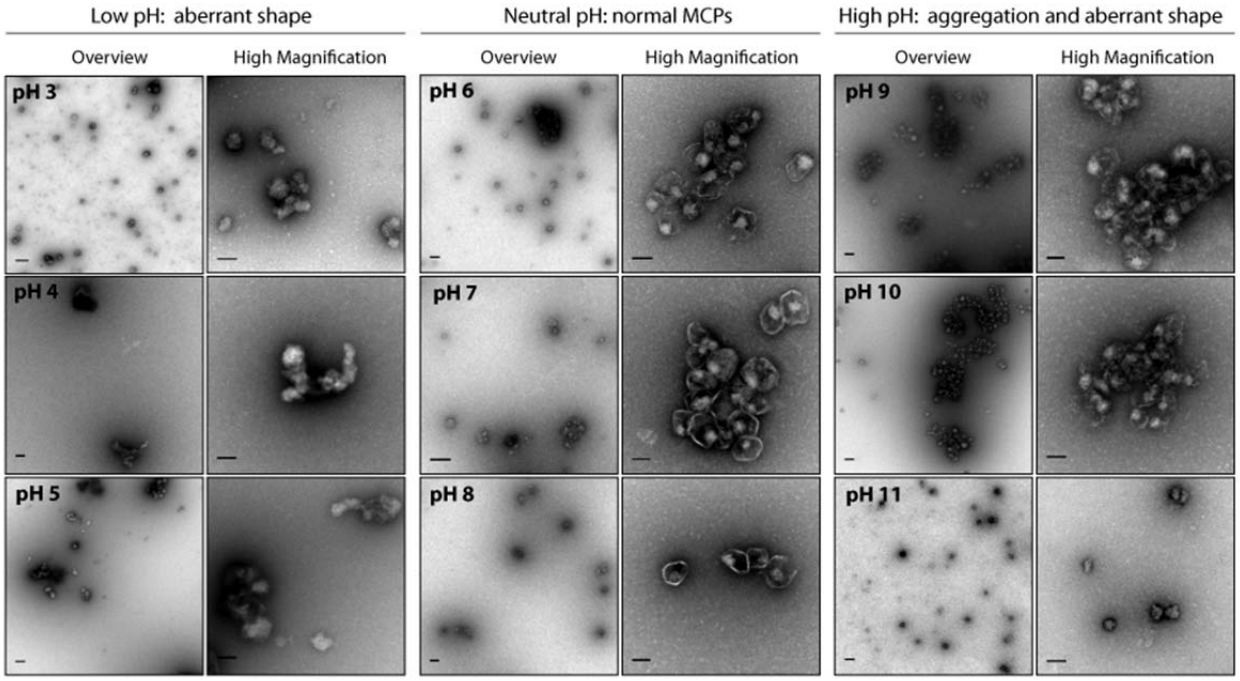


**Figure 2.6: TEM images of purified MCPs in buffers of various pH**
Two representative images are shown for each sample. Scale bars represent 200 nm in overview images, and 100 nm in high magnification images.

As with many proteins, the Pdu MCPs aggregate and denature at high salt conditions. TEM images of MCPs resuspended in 1 M NaCl for two hours show that MCPs have denatured, and outlines of the original MCP bodies cannot be seen (Figure 2.7). Similarly, MCPs are also sensitive to the chaotropic agent urea, and TEM images show that MCPs resuspended in 1 M urea for two hours have denatured.

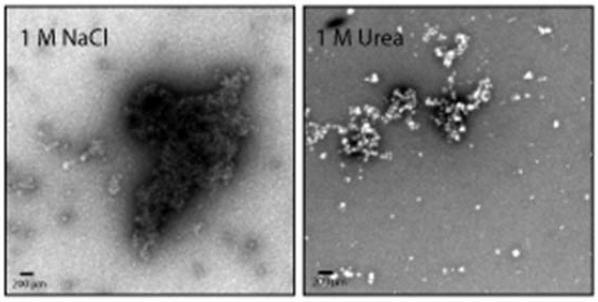


Figure 2.7: TEM images of purified MCPs in high salt and urea

## 2.4 Discussion and Future Directions

We show that the Pdu MCP, like many other capsid systems, is remarkably stable over time and at elevated temperatures. MCPs are able to retain their structure for over one week at 4°C or at room temperature *in vivo* and *in vitro*, and can endure temperatures up to 60°C without any visible aberrations to the shell structure. These findings demonstrate that MCPs are suitable for a diversity of applications. For example, the use of MCPs as *in vivo* nanobioreactors can be expanded to thermophilic organisms incubated at elevated temperatures.

While MCPs are stable, we do observe an increased amount of aggregation at elevated temperatures. However, individual MCP bodies often appear intact within aggregates. We hypothesize that the mechanism for aggregation is the partial unfolding of individual shell proteins, which exposes hydrophobic patches on the MCP surface. An energetically favorable state is created when multiple MCPs come together to bury these hydrophobic patches. The Thermofluor assay could be modified to examine this hypothesis.

We have already used the Thermofluor assay to show that the melting temperature of MCPs is 52.1°C. However, this temperature describes the melting temperature for whole MCPs. As the Pdu MCP shell is made up of nine different proteins, it is possible that some shell proteins may be more stable than others. If this is the case, the denaturation process may lead to the selected denaturation of certain shell proteins first, creating intermediate structures with decreased size or alternate shapes. To address this question, one could measure the melting temperatures of individual shell proteins.

We show that MCPs are sensitive to pH and require an environment between pH 6 and pH 10. However, the disruption of the MCP shell below pH 6 may prove to be a useful mechanism for drug delivery. As many cells uptake targeted protein therapeutics into endosomes, endosomal escape remains a major challenge for effective drug delivery. MCP-based systems can exploit the lowered pH in maturing endosomes, which can reach as low as pH 5, to disassemble and release its cargo [62-64].

We are also interested in the mechanism of MCP disassembly at non-physiological pH. At pH 10, we observe bodies that appear ordered but smaller than the typical 150 nm Pdu MCP, again leading to the concept that intermediate structures may exist from the selected denaturation of individual shell proteins. Similar aberrant bodies are observed when MCPs are incubated in 1 M NaCl or 1 M urea. On the other hand, MCPs incubated at pH 5 and below show aberrant bodies that are less regular and have less defined edges. This may indicate a different mode of MCP denaturation, or a more complete denaturation of all shell proteins.

Finally, an *in vivo* time course using fluorescence microscopy reveals that MCPs can persist for many days in the cytoplasm. The fact that MCPs persist longer than the doubling time of its host organism raises the question of how MCPs segregate to daughter cells, and whether the process is organized or stochastic. Studies on the carboxysome show that segregation is highly ordered and each daughter cell receives an equal amount of carboxysomes [65]. This equal distribution is critical for the fitness of each daughter cell, as carboxysomes are essential for carbon fixation in cyanobacteria. On the other hand, the Pdu MCP does not show such spatial organization

within the cell, and no studies have shown equal partitioning of MCPs to daughter cells. Another unanswered question is whether new Pdu MCPs are formed from existing MCPs, or created *de novo*. In the former case, partitioning of at least one Pdu MCP is essential for each daughter cell to survive. To address some of these questions, it would be interesting to study the time required for MCP formation using time-lapse fluorescence microscopy, and to track MCP position during cell division.

Towards further elucidating the MCP formation process, we are also interested in using the methods developed above, such as DLS, to investigate whether individually purified shell proteins can self-assemble *in vitro*. Such a study would provide insight towards the how MCPs assemble and whether chaperones are required for MCP formation. Furthermore, the possibility of *in vitro* assembly would greatly expand the types of molecules that can be loaded into MCPs. This would be especially useful for drug delivery applications which may require covalent chemical modifications to MCPs.

We have shown that the Pdu MCP is an extremely robust and promising platform for many applications in biotechnology and biomedicine, and established methods for analyzing these and future, engineered, MCP structures.

# Chapter 3: REGULATION OF PDU MCP FORMATION

## 3.1 Introduction

Microcompartments (MCPs) are a mechanism utilized by bacteria to organize and sequester enzymes and the biochemical pathways they catalyze [46, 47]. Various different types of bacterial MCP systems share a general arrangement of an outer protein shell, made up of thousands of subunits, containing encapsulated metabolic enzymes within its lumen. The propanediol utilization (Pdu) MCP, found in several species of enteric bacteria, encapsulates enzymes involved in the utilization of 1,2-propanediol (1,2-PD) as a carbon source. It is thought that the purpose of encapsulating this metabolic pathway is to insulate the cell from the toxic intermediate propionaldehyde [45]. It is to be noted, however, that synthesizing the thousands of proteins that make up the Pdu MCP comes at a high energy cost. Therefore, limiting MCP formation to environments containing 1,2-PD, in which the MCP function is required, is critical for cell fitness. In fact, this requirement of a specific metabolite has kept the Pdu MCP elusive to biologists for many years despite its presence in many well-studied organisms such as *S. enterica*.

There has been growing interest in recent years to utilize MCPs as nanobioreactors by encapsulating engineered synthetic pathways. To do so, it will become necessary to understand the regulatory mechanism behind MCP formation. Previous studies on the regulation of the closely linked cobalamin (vitamin $B_{12}$) biosynthesis pathway first identified that 1,2-PD is a positive effector of transcription of the *pdu* genes in *S. enterica* [66]. In a proposed model for *pdu* regulation, the *pdu* operon is activated by the transcription factor PocR, which is allosterically activated by 1,2-PD. Transcription of the *pocR* gene is under the control of the cAMP receptor protein (Crp) and anoxic redox control (Arc) global regulatory systems [66-69], suggesting that a poor carbon source is required. Here, we continue to investigate the transcriptional regulation of the *pdu* operon. We first find that that 1,2-PD can induce transcription of the *pdu* operon both in minimal and rich media. We then show that heterologous expression of PocR can activate the *pdu* operon to form MCPs in the absence of 1,2-PD. Finally, we express the nine Pdu shell proteins and show that Pdu MCPs can be formed heterologously in *E. coli*.

## 3.2 Materials and Methods

### *3.2.1 Bacterial Strains, Media, and Growth Conditions*

The bacterial strains used in this study are *Escherichia coli* DH10B and *Salmonella enterica* serovar Typhimurium LT2. Cultures were grown in 2 ml of LB Miller medium overnight supplemented with the appropriate antibiotic to maintain the plasmid (34 μg/ml chloramphenicol, 50 μg/ml carbenicillin, or 50 μg/ml kanamycin). For growth in rich media, cultures were diluted 1:100 into 400 ml of lysogeny broth (LB Miller) supplemented with the appropriate antibiotic. For growth in minimal media, cultures were diluted 1:1000 into 400 ml of no-carbon-E (NCE)

minimal medium [57], supplemented with 1 mM MgSO4, 50 μM ferric citrate, and 0.5% succinate in a 2 L flask, supplemented with half the amount of appropriate antibiotic. In cases where MCP formation under natural induction was desired, cultures were supplemented with 0.4% 1,2-propanediol.

All cultures were grown at 37°C in an orbital shaker at 225 rpm. For experiments with gene expression from a plasmid, genes were induced at $OD_{600}$=0.4 with 0.02% arabinose and the specified amount of anhydrotetracycline (aTc). After five additional hours of growth, samples were taken for fluorescence microscopy, and the rest of the cell culture was harvested by centrifugation for Pdu MCP purification.

### *3.2.2 Fluorescence microscopy*

Bacteria were viewed using a Nikon Ni-U upright microscope with a 100x , 1.45 n.a. plan apochromat objective. Images were captured using an Andor Clara-Lite digital camera. Fluorescence images were collected using a C-FL Endow GFP HYQ band pass filter.

### *3.2.3 Pdu MCP purification*

The following MCP purification protocol is adapted from a previously described method [36]. Harvested cell pellet was washed in 40 ml of buffer A (50 mM Tris-HCl, 500 mM KCl, 12,5 mM $MgCl_2$, 1.5% 1,2-PD, pH 8.0). Cells were then resuspended in cell lysis buffer consisting of 10 ml buffer A, 15 ml B-PER II, 5 mM β-mercaptoethanol, 1 mM phenylmethanesulfonyl fluoride, 25 mg lysozyme, and 10 units of DNase I (NEB M0303S), and incubated at room temperature for 30 minutes. The cell lysate was clarified twice by centrifugation at 12,000 x g for 5 minutes at 4°C, then passed through a 0.45 μm filter to remove remaining cellular debris. MCPs were pelleted by centrifugation at 21,000 x g for 20 minutes at 4°C, washed with 4 ml of Buffer A and 6 ml of BPER-II, then pelleted again by centrifugation at 21,000 x g for 20 minutes at 4°C. The MCP pellet was resuspended in 300 μl of Buffer B (50 mM Tris-HCl, 50 mM KCl, 5 mM $MgCl_2$, 1% 1,2-PD, pH 8.0). Remaining debris was removed by three additional centrifugation steps at 12,000 x g for 1 minute at 4°C.

### *3.2.4* Electron microscopy

10 μl of purified MCPs, at a concentration of 100 μg/ml, were placed on 400 mesh formvar coated copper grids with a carbon film for two minutes. The grids were washed three times with deionized water, then stained with 2% aqueous uranyl acetate for two minutes. Samples were observed and photographed with a FEI Tecnai T12 transmission electron microscope.

### *3.2.5 Construction of transcriptional fusions*

To create the $P_{pdu}$-GFP transcriptional fusion, 373 base pairs upstream (5') of the *pduA* start codon was cloned from the genome of *S. enterica* serovar Typhimurium LT2 to capture the putative $P_{pdu}$ promoter, and placed into a pPROTet plasmid. A *gfp* reporter gene, which contains

its own Shine-Dalgarno sequence and start codon, was cloned downstream of the $P_{pdu}$ promoter on the 3' end.

To create the $P_{pocR}$-GFP transcriptional fusion, a similar plasmid was constructed in which the 301 base pairs upstream (5') of the *pocR* start codon was cloned from the genome of *S. enterica* serovar Typhimurium LT2 and placed into a pPROTet plasmid, with a *gfp* reporter cloned downstream (3').

### *3.2.6 Flow cytometry*

For experiments in which $P_{pdu}$ was induced by 1,2-PD, cultures were grown overnight in LB media without 1,2-PD and subcultured 1:100 into the appropriate media for the study. For experiments in which $P_{pdu}$ was induced by heterologous expression of PocR, cultures were grown for additional time until $OD_{600}$=0.4, at which point anhydrous tetracycline (aTc) was added at a concentration of 1 ng/ml to induce PocR expression. At the indicated time points, aliquots of each sample were diluted to an $OD_{600}$ of 0.01 into 200 µl phosphate-buffered saline (PBS) with 2 mg/ml kanamycin to halt translation. These dilutions were then further diluted 1:20 into 200 µl of phosphate-buffered saline with 2 mg/mL kanamycin in 96-well plates. The GFP fluorophore was allowed to mature for 30 minutes following dilution of the final time point, and 10,000 events were collected for each sample on a Millipore Guava easyCyte 5HT flow cytometer. The software FlowJo was used to set a gate around the cell population using the forward and side scatter channels, and average fluorescence values were calculated using the geometric mean.

## 3.3 Results

### *3.3.1 Development of a reporter for pdu transcription*

To investigate regulation of the *pdu* operon, we first constructed a reporter for *pdu* transcription via a transcriptional fusion plasmid in which expression of green fluorescent protein (GFP) is driven by induction of the $P_{pdu}$ promoter ($P_{pdu}$-GFP). We first use this reporter to verify that 1,2-PD activates the pdu operon. Flow cytometry shows that 1,2-PD activates $P_{pdu}$ as early as two hours after induction, and continues over the course of several hours (Figure 3.1). Fluorescence microscopy of *S. enterica* expressing $PduP^{1-18}$-GFP, in which the formation of MCPs is monitored by the emergence of punctate fluorescence from the encapsulated reporter, shows agreement with the flow cytometry results (Figure 3.2). In these images, a small population of cells contains MCPs within three hours after the introduction of 1,2-PD. After four hours, the majority of the cell population contains MCPs.

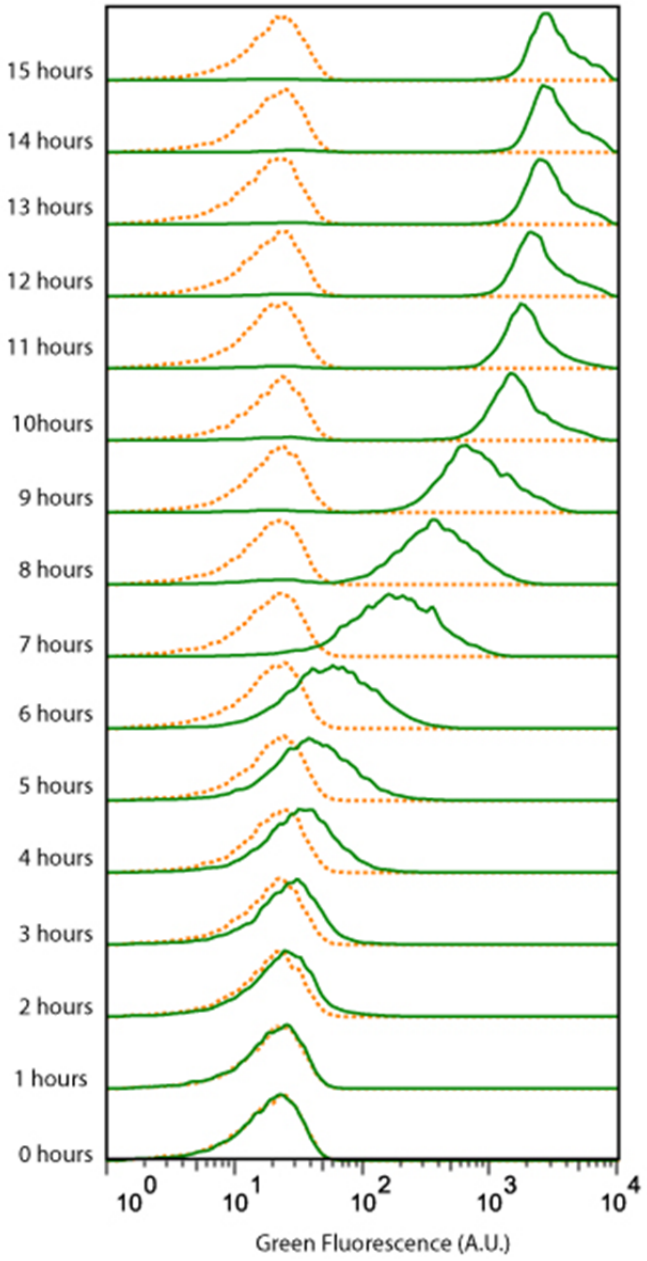


**Figure 3.1: Time course of $P_{pdu}$ induction in NCE minimal media with 1,2-PD**
A transcriptional fusion plasmid was constructed in which expression of a gfp reporter is driven by the $P_{pdu}$ promoter ($P_{pdu}$-GFP). A histogram of green fluorescence, as measured by flow cytometry, is shown over a time course of fifteen hours. The indicated time is the number of hours after cultures of *S. enterica* have been induced with 1,2-PD (solid green lines). Fluorescence from cultures without the addition of 1,2-PD are shown for comparison (dotted orange lines).

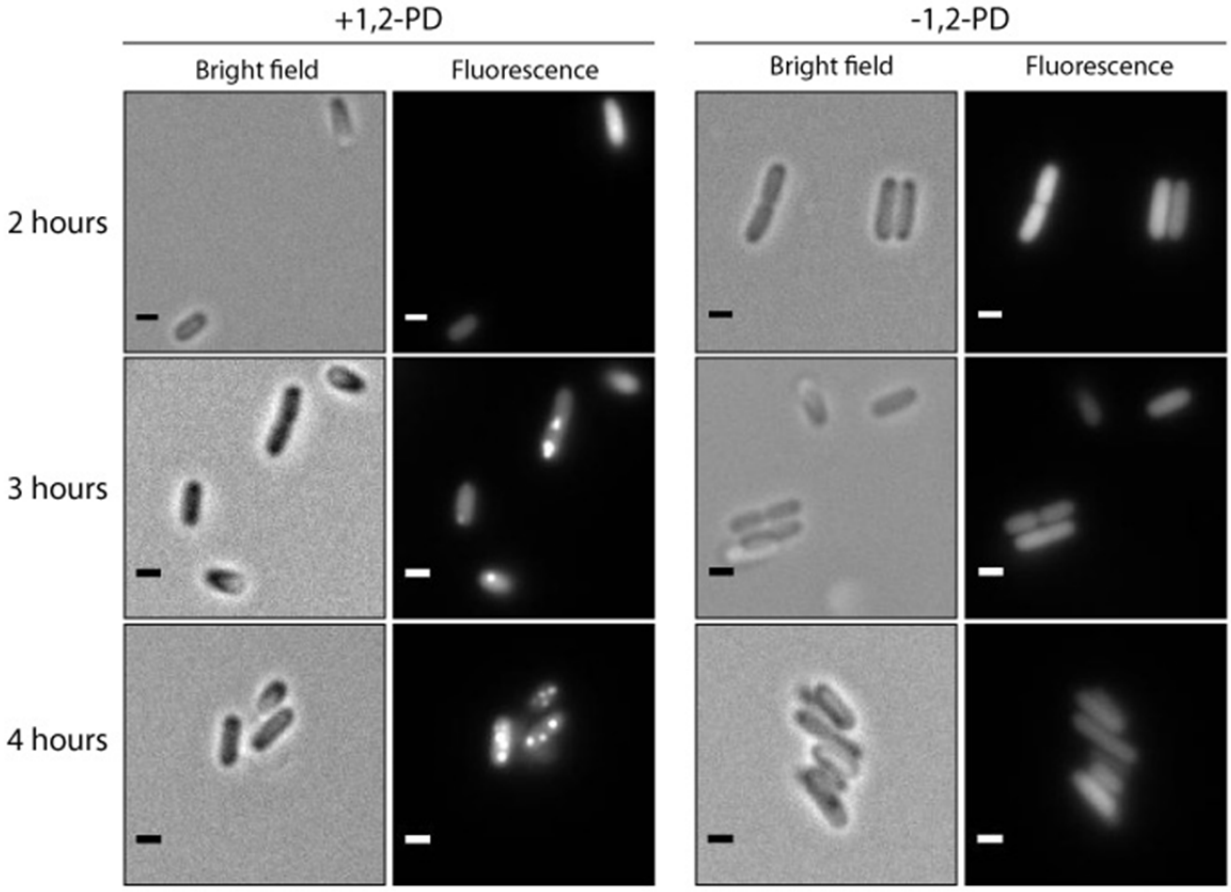


**Figure 3.2: Fluorescence microscopy time course after induction with 1,2-PD**
*S. enterica*, containing a plasmid encoding for $PduP^{1-18}$-GFP, are grown in NCE minimal media. Upon reaching $OD_{600}$=0.4, cultures were induced with 0.02% arabinose for expression of the encapsulated reporter $PduP^{1-18}$-GFP, and 0.4% 1,2-PD to induce MCP formation. Time is given in hours after induction. Scale bars represent 1 μm.

These data show that the $P_{pdu}$-GFP transcriptional fusion plasmid, in combination with flow cytometry, can be a valuable tool for investigating regulation of the *pdu* operon.

### *3.3.2 MCP formation in rich media*

Previous studies report that induction of the Pdu operon requires growth on a poor carbon source [69]. To date, all published work involving endogenous expression of MCPs in *S. enterica* have used NCE minimal media. To investigate the induction of the $P_{pdu}$ promoter in rich media, we once again employ the $P_{pdu}$-GFP transcriptional fusion plasmid. A time course of fluorescence, as measured by flow cytometry, shows that 1,2-PD activates transcription of $P_{pdu}$ in lysogeny broth (LB) Miller (Figure 3.3).

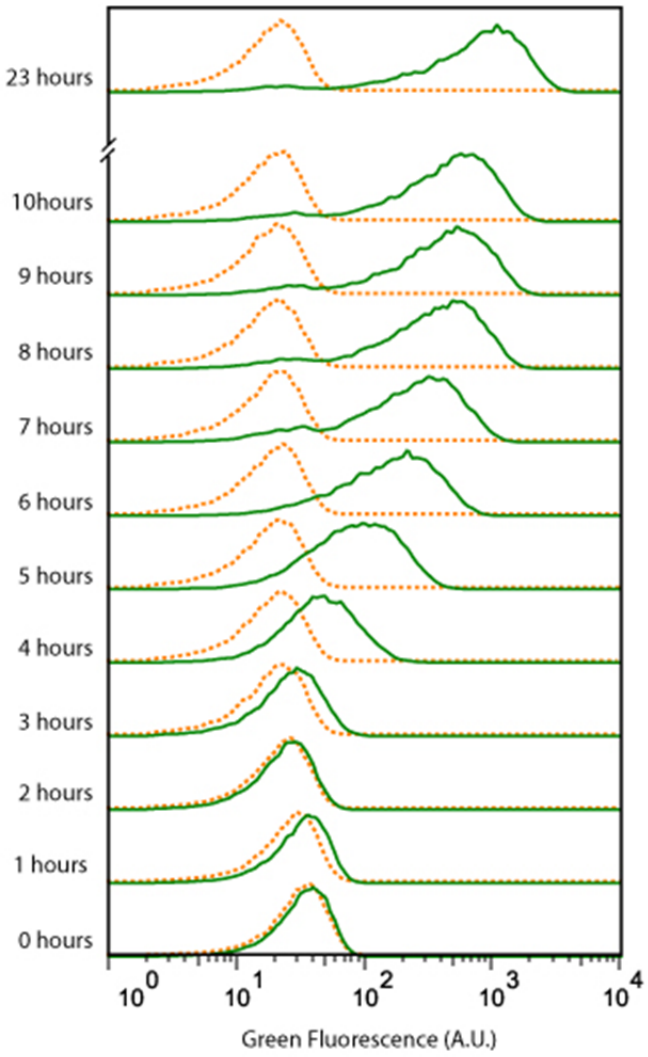


**Figure 3.3: Time course of $P_{pdu}$ induction in LB Miller with 1,2-PD**
A transcriptional fusion plasmid was constructed in which expression of a GFP reporter is driven by the $P_{pdu}$ promoter ($P_{pdu}$-GFP). A histogram of green fluorescence, as measured by flow cytometry, is shown over a time course of several hours. The indicated time is the number of hours after cultures of *S. enterica* have been induced with 1,2-PD (solid green lines). Fluorescence from cultures without the addition of 1,2-PD are shown for comparison (dotted orange lines).

We complement these promoter activation studies with microscopy data showing that MCPs formed in strains grown in LB are morphologically equivalent to MCPs formed in NCE minimal medium. Fluorescence microscopy images show that *S. enterica* grown in LB with added 1,2-PD retain the ability to encapsulate the $PduP^{1-18}$-GFP reporter (Figure 3.4). TEM images from

purified MCPs from *S. enterica* grown in LB and 1,2-PD show no morphological differences when compared to MCPs from the same strain grown in NCE with 1,2-PD (Figure 3.5).

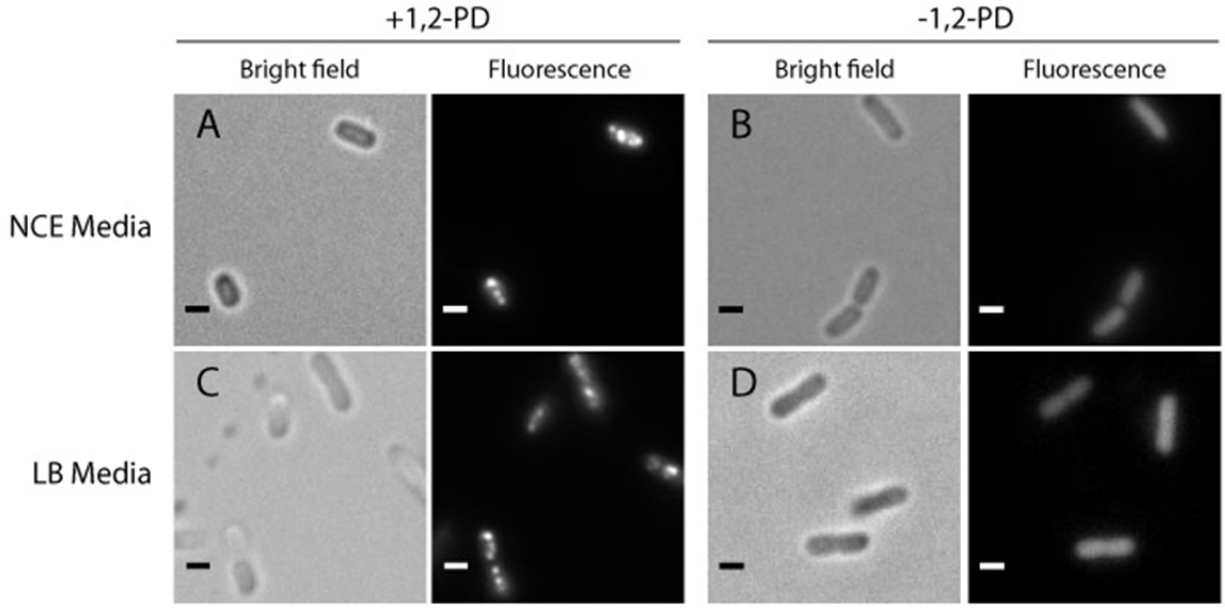


**Figure 3.4: Encapsulation of PduP$^{1-18}$-GFP in different growth media**
*S. enterica* expressing PduP$^{1-18}$-GFP grown in (A) NCE medium with 1,2-PD, (B) NCE medium without 1,2-PD, (C) LB Miller with 1,2-PD, and (D) LB Miller without 1,2-PD. Scale bars represent 1 μm.

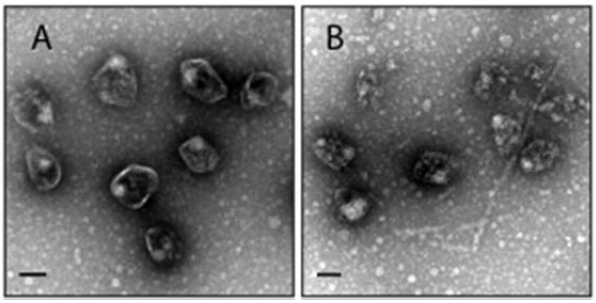


**Figure 3.5: TEM of MCPs from strains grown in different growth media**
MCPs are purified from *S. enterica* expressing PduP$^{1-18}$-GFP grown in (a) NCE medium with 1,2-PD, and (b) LB Miller with 1,2-PD. Scale bars represent 100 nm.

These results indicate that growth in the rich medium LB Miller does not inhibit the endogenous expression of MCPs from *S. enterica*. This may prove useful for the biotechnology community, not only for the wide availability of the media LB, but also due to the higher growth rate of *S. enterica* in LB when compared to NCE minimal media (Figure 3.6).

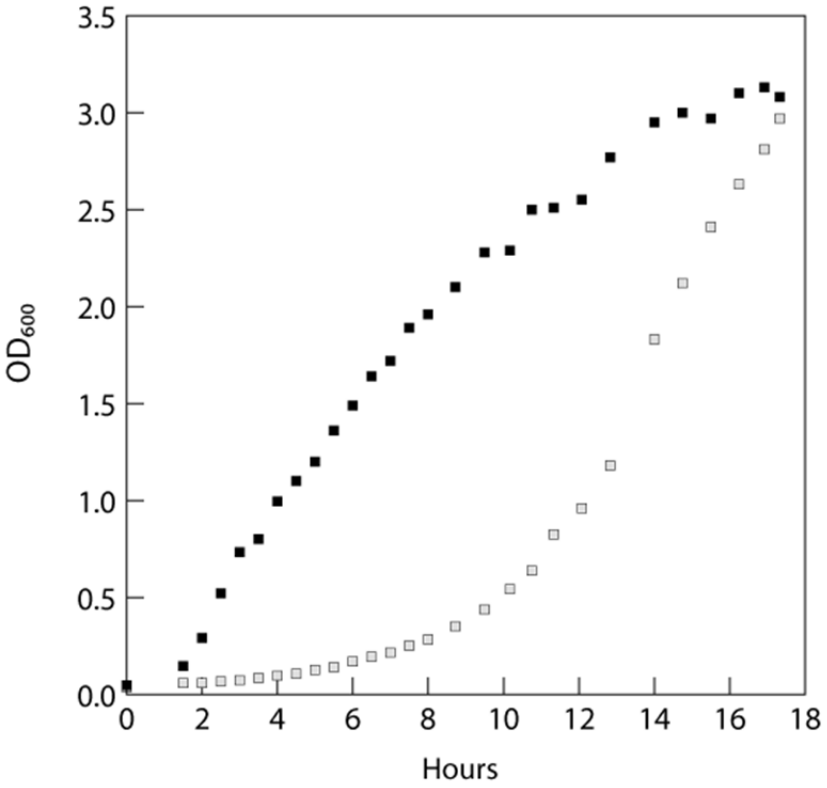


**Figure 3.6: Growth curve of *S. enterica***
*S. enterica* grown in LB Miller (black squares) and NCE minimal medium (open squares).

### *3.3.3 1,2-PD induces transcription of PocR, a transcriptional activator of $P_{pdu}$*

Previous studies report that the $P_{pdu}$ promoter is under positive regulation by transcription factor PocR[66-68]. We directly tested the effects of PocR by monitoring fluorescence from the $P_{pdu}$-GFP transcriptional fusion upon heterologous expression of PocR from an aTc-inducible pTET plasmid. We find that expression of PocR activates the $P_{pdu}$ promoter even in the absence of 1,2-PD (Figure 3.7). This observation is surprising, as it is counter to the current model of allosteric activation of PocR by 1,2-PD.

Next, we show that MCPs formed by heterologous expression of PocR are equivalent to MCPs formed by 1,2-PD induction. Fluorescence microscopy of *S. enterica* grown in LB Miller and co-expressing PocR and $PduP^{1-18}$-GFP shows punctate fluorescence, indicating that MCPs retain the ability to encapsulate proteins (Figure 3.8). TEM images show that MCPs purified from *S. enterica* expressing PocR in the absence of 1,2-PD have no phenotypic aberrations when compared to MCPs formed by 1,2-PD induction (Figure 3.9).

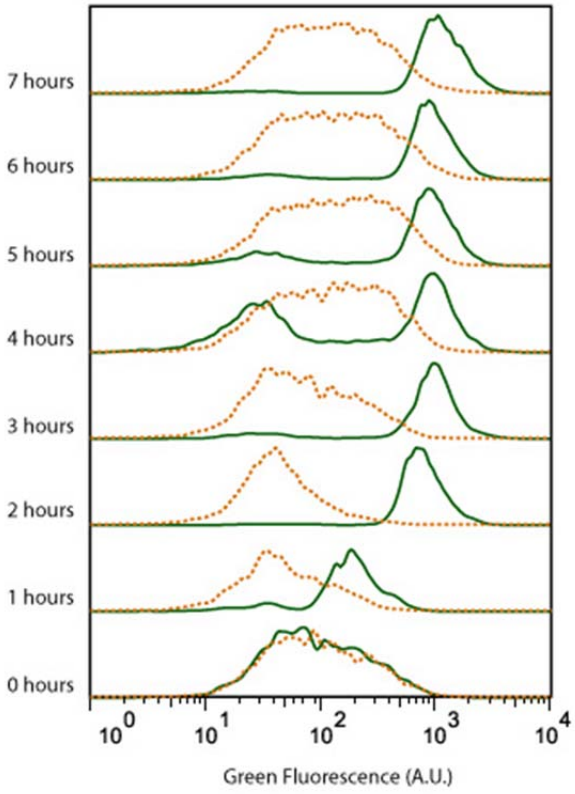


**Figure 3.7: Time course of $P_{pdu}$ induction by transcription factor PocR**
A histogram of green fluorescence, as measured by flow cytometry, is shown over a time course of seven hours. *S. enterica* harboring the $P_{pdu}$-GFP transcription fusion plasmid, and a second aTc-inducible plasmid with PocR, were grown in LB Miller without 1,2-PD. At time 0, cultures of *S. enterica* reached $OD_{600}$=0.4 and continued their growth without added aTc (dotted orange line), or with 4 ng/ml of aTc to induce expression of PocR (solid green line). Cultures without aTc show background fluorescence due to leaky expression of PocR.

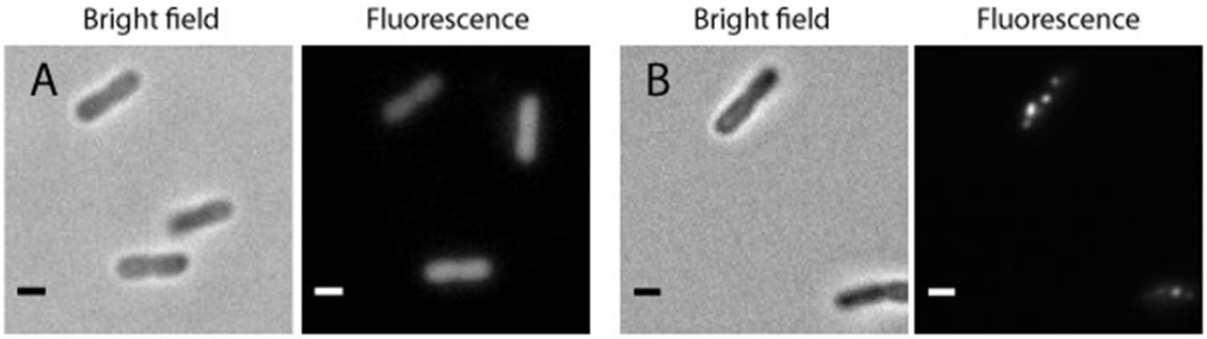


**Figure 3.8: Fluorescence microscopy indicates MCP formation by expression of PocR**
*S. enterica* are grown in LB Miller in the absence of 1,2-PD. Strains express (A) $PduP^{1-18}$-GFP, and (B) co-express $PduP^{1-18}$-GFP and PocR. Scale bars represent 1 μm.

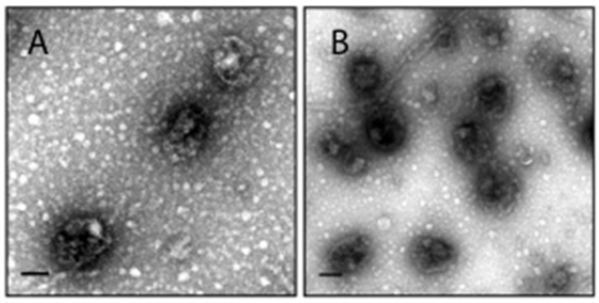


**Figure 3.9: TEM of MCPs from the overexpression of PocR**
MCPs are purified from *S. enterica* expressing PduP$^{1-18}$-GFP grown in (a) LB Miller with 1,2-PD, and (b) LB Miller in the absence of 1,2-PD, with coexpression of PocR. Scale bars represent 100 nm.

### *3.3.4 Heterologous expression of Pdu shell proteins form MCPs in E. coli*

To exploit MCPs as a useful engineering tool, it may desirable to control Pdu MCP formation via a well-characterized inducible promoter system rather than relying on expression by endogenous regulation. Nine Pdu MCP shell protein genes—*pduA, pduB, pduB', pduJ, pduK, pduM, pduN, pduT, pduU*—were cloned into a low copy $P_{TET}$ inducible vector and co-transformed into *E. coli* DH10B with a second plasmid containing the reporter PduP$^{1-18}$-GFP.

Fluorescence microscopy images of *E. coli* expressing the genes from these two plasmids show punctate fluorescence indicative of encapsulated reporter protein within MCPs (Figure 3.10). The overall fluorescence was much greater in *E. coli* compared to *S. enterica*, possibly due to the optimization of the plasmid origin, promoter, and ribosome binding sites for an *E. coli* expression host. In addition, a higher level of background fluorescence is seen within *E. coli* cells, indicative of unencapsulated reporter protein. It is unclear whether this higher level of unencapsulated protein is due to the higher level of overall expression, causing saturation within the MCP, or due to less efficient encapsulation in *E. coli*.

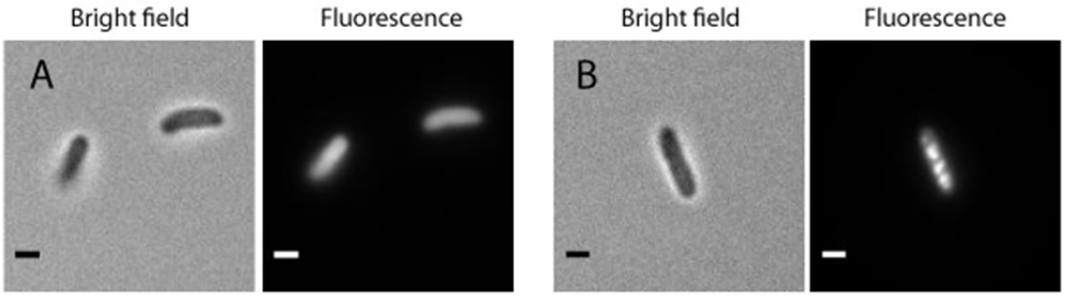


**Figure 3.10: Fluorescence microscopy indicate MCP formation in *E. coli***
*E. coli* are grown in LB Miller (a) expressing PduP$^{1-18}$-GFP, and (b) co-expressing PduP$^{1-18}$-GFP and PduABB'JKMNTU. Scale bars represent 1 μm.

TEM images show that MCPs purified from *E. coli* co-expressing PduP$^{1-18}$-GFP and PduABB'JKMNTU are generally similar to MCPs from wild type *S. enterica* (Figure 3.11). Occasionally, misshapen and elongated MCPs are found (Figure 3.12).

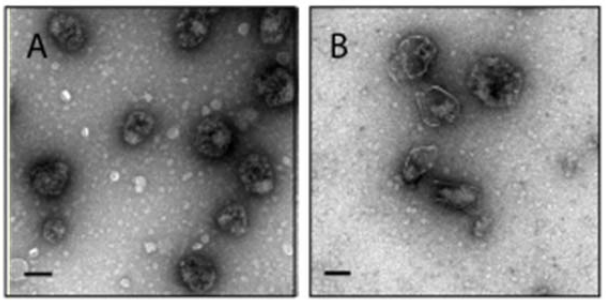


**Figure 3.11: TEM images of MCPs from *S. enterica* and *E. coli***
MCPs are purified from (a) *S. enterica* grown in NCE minimal media with 1,2-PD, and (b) *E. coli* grown in LB Miller, expressing PduP$^{1-18}$-GFP and PduABB'JKMNTU. Scale bars represent 100 nm.

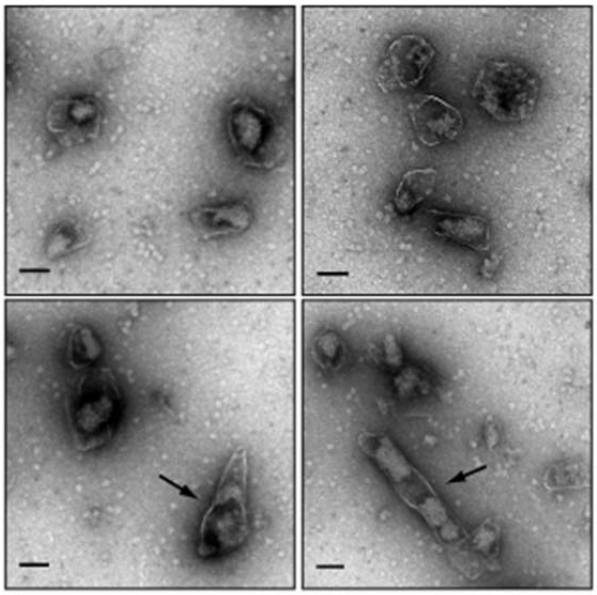

**Figure 3.12: TEM images of MCPs from *E. coli***
MCPs are purified from *E. coli* co-expressing PduABB'JKMNTU and PduP$^{1-18}$-GFP. Arrows highlight MCPs that appear to have morphological deformities. Scale bars represent 100 nm.

To our knowledge, this is the first time that the Pdu MCP has been expressed in *E. coli* in which TEM images show the Pdu MCP to be morphologically similar to those from wild type *S. enterica*. Previous reports by other groups of heterologous expression of the Pdu MCP in *E. coli*

show misshapen MCPs (Figure 3.13), possibly due to incorrect expression levels or incomplete or unbalanced expression of all the shell genes[34, 70].

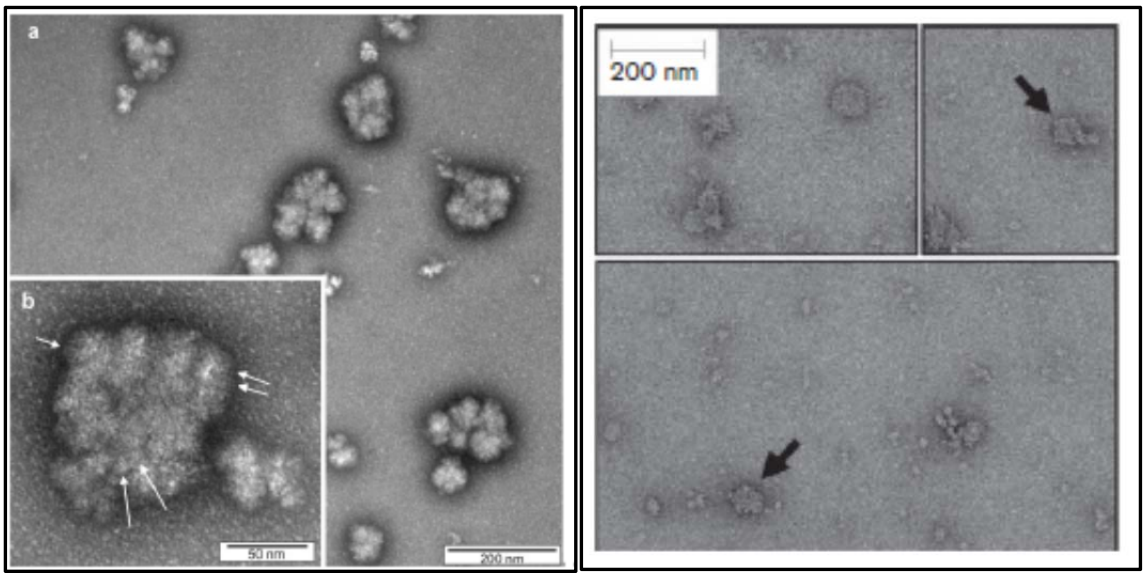


**Figure 3.13: Prior attempts to express Pdu MCPs in *E. coli* by other groups**
(Left) Purified MCPs from *E. coli* containing a cosmid with 30 genes, including the 21 genes of the *pdu* operon [34]. (This research was originally published in *The Journal of Biological Chemistry*. Parsons J. et al, 2008. Vol:283, No. 21, pp 14566-14375. © The American Society for Biochemistry and Molecular Biology.)
(Right) Purified MCPs from *E. coli* co-expressing $PduD^{1-20}$-mCherry and PduABB'TUNJK [70]. (This research was originally published in *Microbiology*. Sargent F. et al, 2013. Vol:159, pp 2427-2436. )

These results show that *E. coli* can be used as a platform for Pdu MCP nanobioreactors. The option to use *E. coli* will greatly expand the availability of the Pdu MCP as a biotechnological tool, as using *S. enterica* as an expression host requires a biosafety level (BSL) 2 biological use authorization, of which many facilities do not have.

## 3.4 Discussion and Future Direction

Prior to this work, the growth conditions used for expression of Pdu MCPs in *S. enterica* often required prior expertise, creating a barrier for new labs entering the field of bacterial MCPs. To highlight this point, the supplements added to NCE minimal media vary in the literature not only among different groups and institutions, but even among publications within the same group. Furthermore, growth in NCE media is slow compared to growth in rich media, making precision timing for induction of heterologous protein difficult. With the construction of a transcriptional fusion reporter plasmid to observe transcription of the *pdu* operon, we present our findings that can alleviate the problems that pose as a barrier for groups studying the Pdu MCP.

First, we show that *S. enterica* may be grown in the LB Miller without inhibiting MCP formation. TEM images show that these MCPs have no apparent morphological differences from MCPs in *S. enterica* grown in previously published growth conditions. Furthermore, fluorescence microscopy supports that encapsulation of $PduP^{1-18}$-GFP is not inhibited. The transcriptional fusion reporter we describe can be used to further test a range of different media types, which will allow for flexibility to choose a growth medium based on the need for faster growth rates, lower cost, or other constraints. While we expect that many different types of rich media allow for MCP formation, preliminary results indicate that glucose is an inhibitor of *pdu* transcription. We are currently investigating the mechanism for this observation.

Next, we show that MCPs can be formed by heterologous expression of the transcriptional activator PocR. While in our studies we used a low concentration of aTc to induce PocR expression, we speculate that an increase in *pocR* expression can increase the number of MCPs formed per cell. This may be beneficial for utilizing MCPs as nanobioreactors, as the total reaction volume per cell is increased.

Finally, we show that the Pdu MCP can be expressed in *E. coli*. While TEM reveals that a small fraction of MCPs appear elongated and misshapen, many MCPs are of similar shape and size to MCPs from *S. enterica*. Working with *E. coli* alleviates the requirement of working in a BSL 2 facility, greatly increasing accessibility of the Pdu MCP. Furthermore, *E. coli* is the most widely studied model organism and therefore has high genetic tractability, leading to many techniques and industrial processes already being well established. The heterologous expression of MCP shell proteins from a plasmid also allows for flexibility in expression levels. In addition to increasing overall expression to increase the number of MCPs per cell, the expression for each individual shell protein can be modulated by modifying Shine-Dalgarno sequences. By changing the ratio of MCP shell protein, it may be possible to create larger MCPs, resulting in increased encapsulation capacity.

We set out to gain an understanding of Pdu MCP regulation. While we have shown that overexpression of the transcriptional activator PocR results in MCP formation, we anticipate future studies will focus on whether PocR is necessary and sufficient for this result. It is also of interest to explore further the regulation of the *pocR* gene from the $P_{pocR}$ promoter.

The insights gained from the regulation of the Pdu MCP are likely generalizable to other MCPs, and may lead to the discovery of new MCP systems. While genetic analysis predicts the existence of many different MCP systems, only three from the bacterial microcompartment family—the carboxysome, Eut, and Pdu MCPs—have been discovered experimentally, likely due to the requirement of a specific metabolite for expression. As an alternative approach to growing various bacteria in a library of metabolites, genomes from bacteria with putative MCPs can be searched for homologs of PocR, and MCPs may be expressed and discovered from the heterologous expression of their regulatory proteins.

Finally, we observe brighter puncta from $PduP^{1-18}$-GFP when grown with both 1,2-PD and expression of PocR than from expression by one of these methods alone. At this time, it is unclear if this is due to differences in expression levels or synergistic effects between 1,2-PD and

PocR expression. The methods described in Chapter 4 will be useful in an exploration of this potential synergy.

# Chapter 4: DEVELOPMENT OF A HIGH-THROUGHPUT ASSAY FOR MCP ENCAPSULATION AND CHARACTERIZATION OF THE PDU MCP TARGETING PEPTIDE

## 4.1 Introduction

Living systems often utilize compartmentalization for the spatial and temporal control of biochemical reactions, as well as providing controlled microenvironments. This strategy is seen in bacterial microcompartments (MCPs) which serve as subcellular organelles in bacteria [46, 47]. Due to the biotechnological interest of producing proteins and biomolecules in bacteria, it has been proposed that bacterial MCPs could be used to encapsulate synthetic metabolic pathways. The encapsulation of these pathways provides numerous potential benefits, including the ability to express pathways that contain toxic intermediates [45], to create custom microenvironments within the MCP that differ from that of the cytosol, and to enhance kinetics through the concentration and colocalization of enzymes involved in a pathway [4].

Recent progress has been made in the characterization of the propanediol utilization microcompartment (Pdu MCP), a naturally occurring MCP system found in *Salmonella enterica* and other enteric bacteria. The Pdu MCP is composed of a protein shell consisting of several thousand protein monomers, of which there are nine different types [21, 23, 34-37, 44]. The protein shell encapsulates enzymes involved in 1,2-propanediol (1,2-PD) catabolism [61]. Because the first two steps of 1,2-PD catabolism occur in the lumen of the MCP, it is thought that the cell is shielded from the toxic propionaldehyde intermediate.

Two proteins naturally encapsulated in the Pdu MCP, PduD and PduP, have N-terminal extensions not seen in non-MCP associated homologs when compared by sequence alignment (Figure 4.1). Fan *et al.* have found that the N-terminal extension from PduP, when fused to the respective heterologous protein, is sufficient to localize green fluorescent protein (GFP), maltose binding protein (MBP), and glutathione S-transferase (GST) to the Pdu MCP [18]. Fusion of the N-terminal region of PduD was also shown to localize heterologous proteins to the Pdu MCP [40]. Furthermore, it was shown that these proteins were encapsulated in the lumen of the MCP rather than simply being associated with the outer faces of the protein shell [18]. The mechanism of encapsulation was found to involve interactions between key amino acid residues in the alpha-helical N-terminal region of PduP and an alpha helix near the C-terminus of the shell protein PduA [42]. A similar mechanism has yet to be reported for the PduD N-terminal region, or for a number of other MCP-encapsulated enzymes such as those in the homologous Eut system.

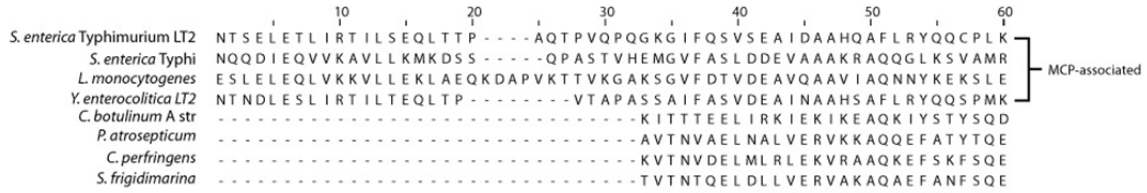


**Figure 4.1: Multiple sequence alignment of a representative sample of PduP homologs**
The alignment shows the first 60 amino acids of four representative MCP-associated PduP homologs and four non MCP-associated PduP homologs. The National Center for Biotechnology Information accession identifications, beginning from the top entry, are 5069459, 16761381, 46907383, 123442957, 148378348, 50121254, 110798574, and 114563069.

A key step towards engineering bacterial MCPs as a biotechnological tool is to reliably control protein encapsulation into MCPs. However, current methods used to detect the level of protein encapsulation within MCPs involve either a time consuming MCP purification and subsequent western blotting, or microscopy of MCP-encapsulated fluorescent proteins, a faster but still low-throughput method [35, 42]. Here, we describe a method for using flow cytometry to detect encapsulated fluorescent proteins. Using this assay, we characterize a library of single amino acid substitution mutants in the signal sequence $PduP^{1-18,}$ with varying encapsulation signaling strength, and identify mutants that encapsulate higher levels of protein compared to the wild type $PduP^{1-18}$ sequence.

## 4.2 Materials and Methods

### 4.2.1 *Bacterial Strains, Media, and Growth Conditions*

The bacterial strain used in this study was *Salmonella enterica* serovar Typhimurium LT2. Cultures were grown in 300 µl LB Miller medium overnight in 96 deep well plates and were diluted 1:1000 into 5 ml of NCE minimal medium supplemented with 1 mM MgSO4, 50 µM ferric citrate, 0.5% succinate, 0.4% 1,2-propanediol, and antibiotic (17 µg/ml chloramphenicol) in 24-well culture plates. Cells were grown at 37°C in an orbital shaker at 225 rpm. At $OD_{600}$=0.4, gene expression was induced with 0.02% arabinose. Cells were incubated for an additional five hours, and then samples were taken for fluorescence microscopy or flow cytometry.

### *4.2.2 Plasmid Construction*

$PduP^{1-18}$-GFP gene fusions were constructed by PCR of GFP mutant 2 [24] with primers containing overhangs containing the first 54 bases of the pduP gene from wild type *S. enterica* serovar Typhimurium LT2. $PduP^{1-18}$-GFP-SsrA was constructed in the same manner but with additional overhangs containing the 33 bases encoding for the SsrA degradation peptide ANDENYALAA. These genes were cloned into a pBAD33 expression vector [25].

### 4.2.3 *Generation of single amino acid substitution library*

PduP$^{1-18}$-GFP-SsrA mutants were constructed by PCR in which the codon for the substituted amino acid was randomized by degenerate NNK primers, where N is an equimolar mixture of all four nucleotides and K is an equimolar mixture of bases G and T. Mutants were cloned into the plasmid pBAD33 using SacI and HindIII restriction sites. To bypass the inherent inefficiency of transforming ligation products into *S. enterica*, the ligations were first transformed into *Escherichia coli* DH10B. The plasmids were purified from the *E. coli* cells and were then used to transform *S. enterica,* generating the library of PduP$^{1-18}$-GFP-SsrA mutants. For each library of single amino acid substitution mutants, 96 colonies were sequenced and analyzed.

### *4.2.4 Fluorescence microscopy*

Bacteria were viewed using a Nikon Ni-U upright microscope with a 100x , 1.45 n.a. plan apochromat objective. Images were captured using an Andor Clara-Lite digital camera. Fluorescence images were collected using a C-FL Endow GFP HYQ band pass filter. The camera exposure time was 50ms for strains expressing fusion proteins without the SsrA tag, and 800ms for strains with the SsrA tag.

### *4.2.5 Western blot*

Purified MCPs were separated by SDS/PAGE using 12.5% (wt/vol) polyacrylamide gels, transferred to PVDF membranes, then detected by western blotting according to standard protocols using non-fat milk as a blocking agent. The antibodies used were anti-GFP (Clontech 632375) at a 1:2000 dilution and horseradish peroxidase-conjugated mouse anti-goat (Thermo Scientific 32430) at a 1:1000 dilution. Chemiluminescence from the substrate SuperSignal West Pico (Pierce 34080SPCL) was detected on a Bio-Rad ChemiDoc XRS+ with an exposure time of 10 minutes.

### *4.2.6 Flow cytometry*

For each mutant, cell cultures were diluted 1:4,000 in 200 µl of phosphate buffered saline in 96-well plates, and 5000 events were collected on a Millipore Guava easyCyte 5HT flow cytometer. The software FlowJo was used to set a gate around the cell population using the forward- and side-scatter channels, and average fluorescence values were calculated using the geometric mean.

### *4.2.7 Pdu MCP purification*

Strains were grown in 400 ml of NCE medium supplemented with 1 mM MgSO4, 0.5% succinate, 0.4% 1,2-PD, and 200 µl of chloramphenicol at 37°C and shaken at 225 rpm. Upon reaching $OD_{600}$=0.4, 0.02% arabinose was added to induce the production of the reporter protein. After five additional hours of growth, cells were harvested by centrifugation. The subsequent MCP purification steps are adapted from a previously described method [36].

Harvested cell pellet was washed in 40 ml of buffer A (50 mM Tris-HCl, 500 mM KCl, 12,5 mM $MgCl_2$, 1.5% 1,2-PD, pH 8.0). Cells were then resuspended in cell lysis buffer consisting of 10 ml buffer A, 15 ml B-PER II, 5 mM β-mercaptoethanol, 1 mM phenylmethanesulfonyl fluoride, 25 mg lysozyme, and 10 units of DNase I (NEB M0303S), and incubated at room temperature for 30 minutes. The cell lysate was clarified twice by centrifugation at 12,000 x g for 5 minutes at 4°C, then passed through a 0.45 μm filter to remove remaining cellular debris. MCPs were pelleted by centrifugation at 21,000 x g for 20 minutes at 4°C, washed with 4 ml of Buffer A and 6 ml of BPER-II, then pelleted again by centrifugation at 21,000 x g for 20 minutes at 4°C. The MCP pellet was resuspended in 300 μl of Buffer B (50 mM Tris-HCl, 50 mM KCl, 5 mM $MgCl_2$, 1% 1,2-PD, pH 8.0). Remaining debris was removed by three additional centrifugation steps at 12,000 x g for 1 minute at 4°C.

#### 4.2.8 *Electron microscopy*

10 μl of purified MCPs were placed on 400 mesh formvar coated copper grids with a carbon film for two minutes. The grids were washed three times with deionized water, then stained with 2% aqueous uranyl acetate for one minute. Samples were observed and photographed with a FEI Tecnai T12 transmission electron microscope.

## 4.3 Results

### *4.3.1 Bioinformatics*

A bioinformatics study by Fan *et. al* have identified a set of putative MCP-associated homologs of PduP. We first carry out a multiple sequence alignment of the first 20 amino acids of MCP-associated homologs of PduP. The alignment reveals a pattern of highly conserved hydrophobic residues spaced between charged amino acids. A Wenxiang projection reveals that the hydrophobic residues align to once side of the alpha helix, possibly indicating a site for binding for burial of the hydrophobic face. However, to gain additional insight on the relationship between amino acid sequence and the ability to encapsulate proteins, it will first be necessary to develop a high throughput method for detecting encapsulation of proteins.

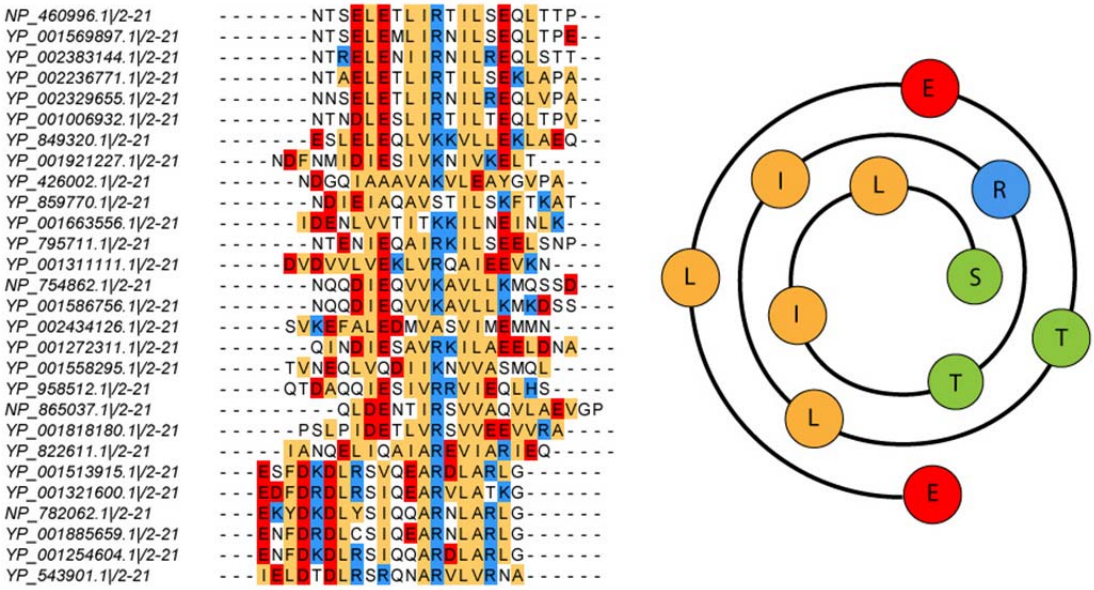


**Figure 4.2: Multiple sequence alignment of the MCP-associated PduP homologs**
(Left) The first 20 amino acids of MCP-associated homologs of PduP are aligned using the MAFFT algorithm [71]. Positively charged amino acid residues are highlighted in red, negatively charged residues in blue, and hydrophobic residues in yellow.
(Right) A Wenxiang diagram projects the alpha helical PduP signal sequence from *S. enterica* serovar Typhimurium LT2, starting at residue 5 on the outside, to residue 15 in the center. Positively charged amino acid residues are highlighted in red, negatively charged residues in blue, hydrophobic residues in yellow, and polar residues in green.

### *4.3.2 Development of an in vivo assay for encapsulation into the Pdu MCP*

We have developed a flow cytometry assay that utilizes fluorescent proteins to quantify the efficiency of protein encapsulation within MCPs. A gene fusion was constructed with the N-terminal encapsulation signal sequence PduP$^{1-18}$, the fluorescent reporter GFP, and a C-terminal SsrA tag to create PduP$^{1-18}$-GFP-SsrA, and placed in a pBAD33 expression vector. The addition of the short SsrA peptide targets cytosolic proteins for degradation by the ClpXP and ClpAP proteases [72-74]. Successful encapsulation of PduP$^{1-18}$-GFP-SsrA protects the fusion protein from degradation due to the inability of the proteases to access the SsrA-tagged substrate (Figure 4.3).

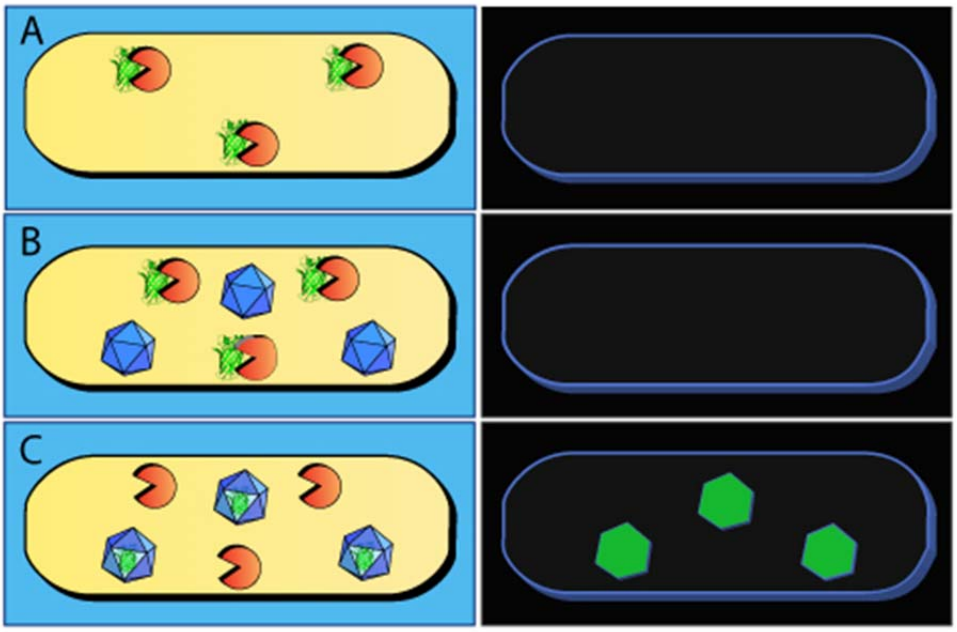


**Figure 4.3: Diagram of the protein encapsulation flow cytometry assay.**
*S. enterica* expresses PduP$^{1-18}$-GFP-SsrA (green barrels). (A) Without the formation of Pdu MCPs, the fusion protein is degraded by the ClpXP protease (orange). (B) In the presence of Pdu MCPs, the fusion protein is degraded if not localized to the Pdu microcompartments. (C) The localization of the fusion protein to the lumen of the Pdu MCPs result in fluorescence due to the inability of the ClpXP protease to access and degrade the fusion protein.

When visualized by microscopy, cells expressing PduP$^{1-18}$-GFP-SsrA in the presence of 1,2-PD have punctate fluorescence similar to cells expressing PduP$^{1-18}$-GFP, although with less overall fluorescence intensity (Figure 4.4 A, C). When grown in the absence of 1,2-PD, MCPs do not form and fluorescence in cells expressing PduP$^{1-18}$-GFP appear diffuse, while cells expressing PduP$^{1-18}$-GFP-SsrA have minimal fluorescence due to the degradation of the cytosol-localized fusion protein (Figure 4.4 B,D). It should be noted that cells expressing GFP without any tags display diffuse fluorescence and cells expressing GFP-SsrA have minimal fluorescence when grown with or without 1,2-PD (Figure 4.4 E, F). The degradation of cytosolic fusion protein allows for the coupling of the quantity of MCP-encapsulated PduP$^{1-18}$-GFP-SsrA with total cellular fluorescence. Flow cytometry can then be used to measure the fluorescence in a high-throughput automated process. This strategy has previously been used in the development of a high-throughput assay for protein export [75]. An added benefit from this flow cytometry assay is the ability to quantify the amount of protein encapsulated into MCPs, whereas microscopy-based methods only qualitatively detect whether proteins are or are not encapsulated within the MCPs [18, 34, 35, 38].

We first applied this assay to assess the ability of wild-type PduP$^{1-18}$ to encapsulate GFP-SsrA, along with two alanine-substitution mutants which have previously been shown to retain (PduP$^{1-18}$S4A) or abolish (PduP$^{1-18}$I10A) the ability to target proteins to the Pdu MCP[42]. Microscopy of *S. enterica* LT2 expressing these fusion proteins indicated that PduP$^{1-18}$-GFP-SsrA and PduP$^{1-}$

$^{18}$S4A-GFP-SsrA are encapsulated while PduP$^{1-18}$I10A-GFP-SsrA was unable to encapsulate within MCPs (Figure 4.4 G, H).

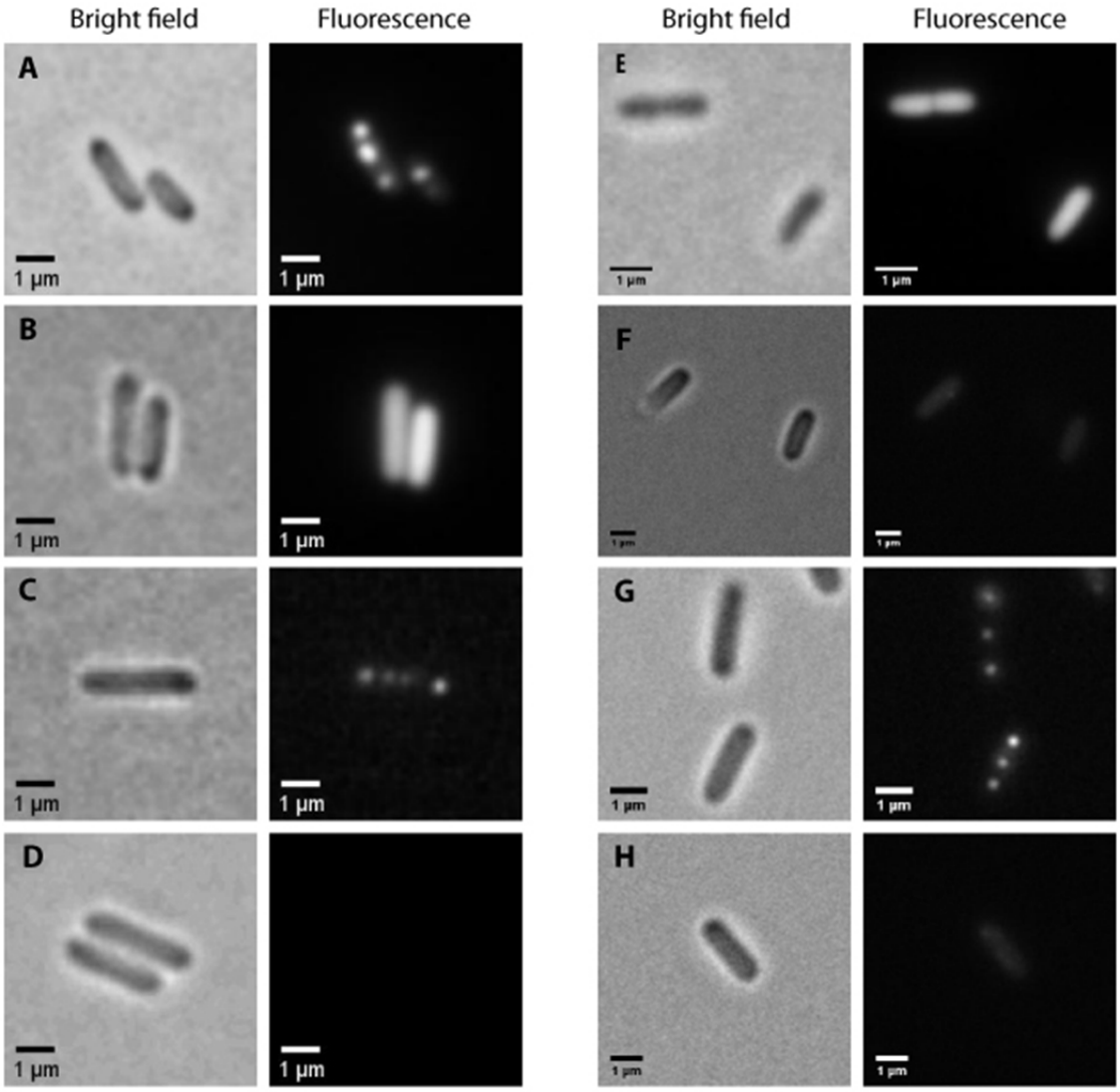


**Figure 4.4: Bright field and fluorescence microscopy MCP-encapsulated GFP**
Encapsulated GFP appear as bright fluorescent puncta in *S. enterica*. Cells are expressing (A) PduP$^{1-18}$-GFP, (B) PduP$^{1-18}$-GFP in the absence of 1,2-PD, (C) PduP$^{1-18}$-GFP-SsrA, (D) PduP$^{1-18}$-GFP-SsrA in the absence of 1,2-PD, (E) GFP, (F) GFP-SsrA, (G) PduP$^{1-18}$S4A-GFP-SsrA, and (H) PduP$^{1-18}$I10A-GFP-SsrA. The camera exposure time was 50ms for strains expressing fusion proteins without the SsrA tag, and 800ms for strains with the SsrA tag.

When these three strains are examined by flow cytometry, we observe a shift in fluorescence for cell populations expressing the fusion proteins with encapsulation-competent PduP$^{1-18}$ and PduP$^{1-18}$S4A signal sequences when compared to cells expressing the same constructs in the absence of 1,2-PD (Figure 4.5 A, B). For cells expressing the fusion protein with the non-

encapsulating PduP$^{1-18}$I10A signal sequence, no shift in fluorescence is observed (Figure 4.5 C). The ratio of the mean fluorescence in cells grown with 1,2-PD over the mean fluorescence of cells grown in the absence of 1,2-PD gives an indication of the level of protein encapsulation, with higher ratios indicating more protein encapsulated, and ratios near one indicating poor encapsulation. These ratios are 1,32, 1.44, and 1.05 for PduP$^{1-18}$, PduP$^{1-18}$S4A, and PduP$^{1-18}$I10A, respectively.

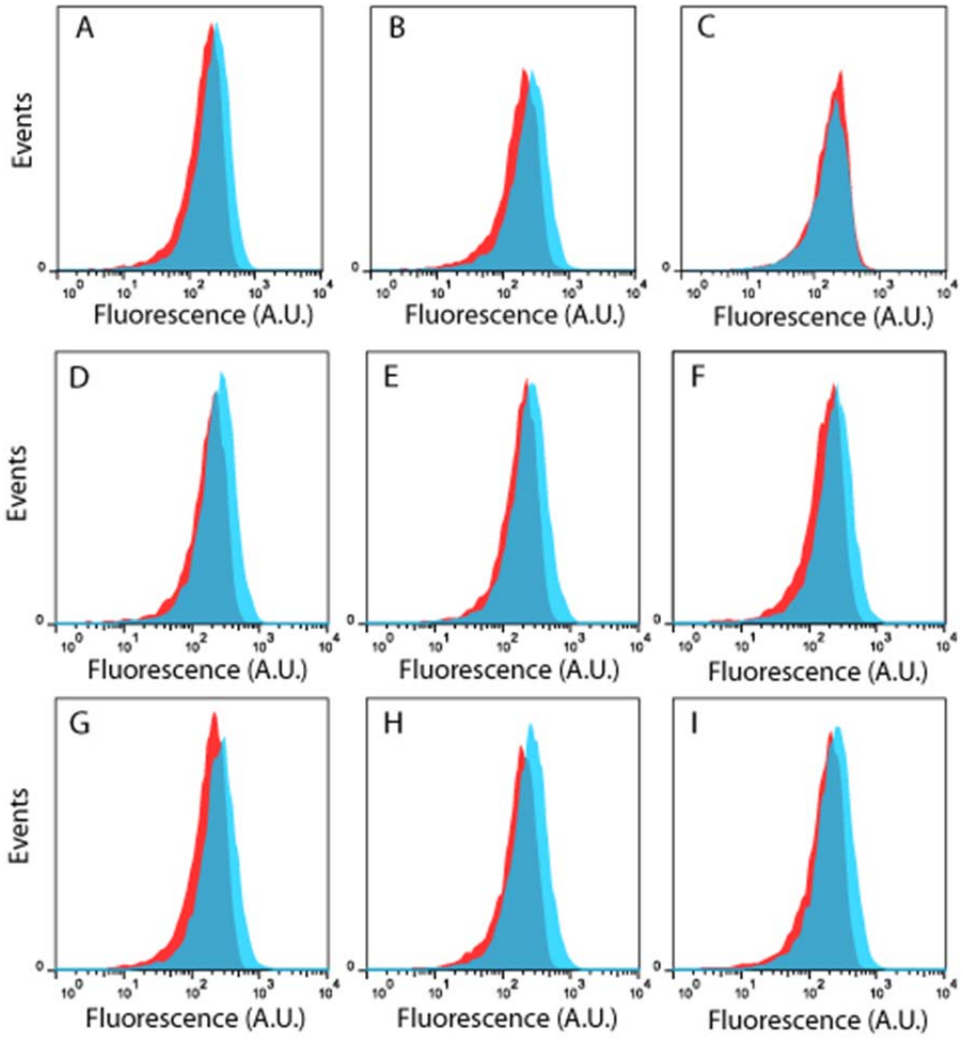


**Figure 4.5: Flow cytometry histograms for GFP encapsulation**
Flow cytometry histograms show a shift in green fluorescence for *S. enterica* expressing MCP encapsulation-competent (A) PduP$^{1-18}$-GFP-SsrA and (B) PduP$^{1-18}$S4A-GFP-SsrA when compared to cells grown in the absence of MCP-inducing 1,2-PD. No shift in green fluorescence was observed for the non-encapsulating (C) PduP$^{1-18}$I10A-GFP-SsrA. While the shift in fluorescence for encapsulated PduP$^{1-18}$-GFP-SsrA is slight, it is reproducible (D-I). The blue curve represents cells grown in media containing 1,2-PD, and red curves in media without 1,2-PD.

A western blot of purified MCPs from these strains confirms the flow cytometry results (Figure 4.6). Importantly, transmission electron micrographs reveal that purified MCPs from cells expressing PduP$^{1-18}$I10A-GFP-SsrA are structurally similar to MCPs from strains not expressing the fusion protein, indicating that the lack of fluorescence is not due to malformation of MCPs (Figure 4.7). Taken together, these results show that this assay can be used to assess protein encapsulation within MCPs.

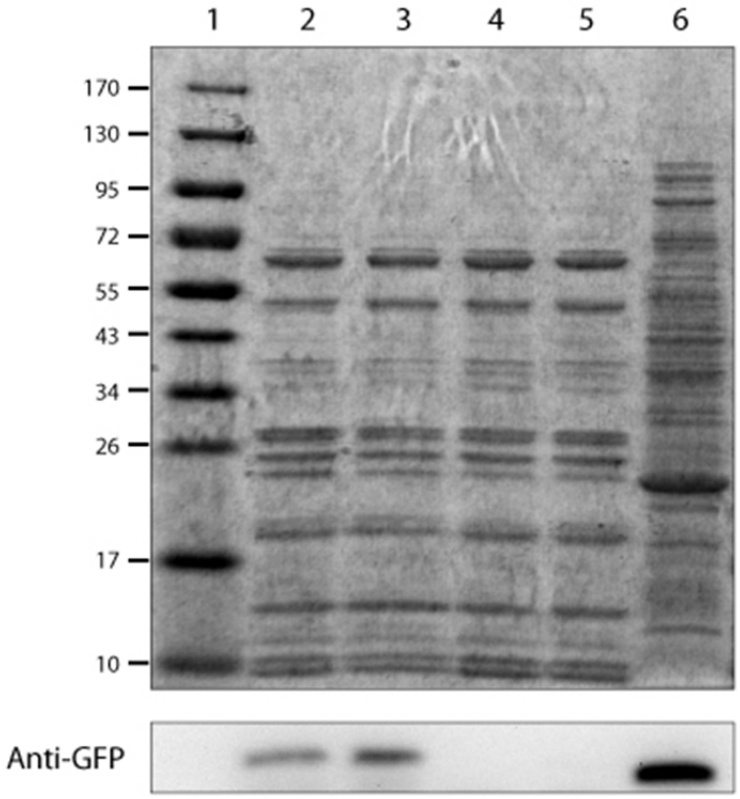


**Figure 4.6: SDS-PAGE gel and Anti-GFP western blot of purified MCPs**
4%-20% SDS-PAGE gel and anti-GFP western blot of a (lane 1) molecular mass marker, and purified MCPs from *S. enterica* expressing (lane 2) PduP$^{1-18}$-GFP-SsrA, (lane 3) PduP$^{1-18}$S4A-GFP-SsrA, (lane 4) PduP$^{1-18}$I10A-GFP-SsrA, and (lane 5) GFP-SsrA, along with cell lysate from *S. enterica* expressing PduP$^{1-18}$-GFP (Lane 6). Lanes with purified MCPs were loaded with 10 μg of total protein.

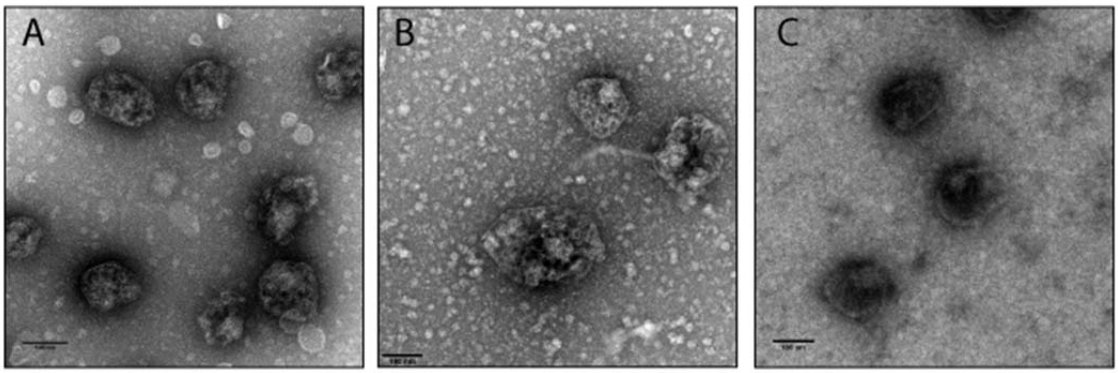


**Figure 4.7: Transmission electron micrographs of purified MCPs**
Transmission electron micrographs of purified compartments from (A) *Salmonella typhimurium* LT2, expressing (B) PduP$^{1-18}$-GFP-SsrA, and (C) PduP$^{1-18}$I10A-GFP-SsrA. No observable aberrations in MCP shell structure in cells expressing the fusion protein with a mutated signal sequence. Scale bars represent 100 nm.

### *4.3.3 Alanine scan of PduP$^{1-18}$*

We expanded the flow cytometry assay to carry out a full alanine scan of PduP$^{1-18}$-GFP-SsrA, and compared these results to those obtained using fluorescence microscopy with cells expressing constructs without a degradation tag. We first constructed each alanine mutation in the PduP$^{1-18}$ signal sequence and visualized compartmentalization of the resulting PduP$^{1-18}$-GFP mutant library with fluorescence microscopy (Table 4.1 and Figure 4.8). Our data exhibits some deviations from what is previously reported by Fan *et al*., who performed an alanine scan on the signal sequence using full-length PduP as a reporter with *in vitro* assays [42]. For instance, in our hands, PduP$^{1-18}$E7A-GFP compartmentalizes while PduP$^{1-18}$I13A-GFP does not compartmentalize. The most notable of our deviations, however, is that we do not see the discrete all-or-nothing encapsulation of proteins previously reported. For example, several mutations (L6A, L9A, and L14A) display limited encapsulation, marked by high fluorescent background in the cytosol with faint but observable fluorescent puncta. These findings provide an excellent test case for the application of the flow cytometry assay to measure the level of protein encapsulation in MCPs.

| **PduP$^{1-18}$ single amino acid alanine substitution** | | | | | | | | | | | | | | | | | |
|---|---|---|---|---|---|---|---|---|---|---|---|---|---|---|---|---|---|
| 1 | 2 | 3 | 4 | 5 | 6 | 7 | 8 | 9 | 10 | 11 | 12 | 13 | 14 | 15 | 16 | 17 | 18 |
| M | N | T | S | E | L | E | T | L | I | R | T | I | L | S | E | Q | L |
| | + | + | + | + | -* | + | + | -* | - | + | + | - | -* | + | + | + | + |

**Table 4.1: Summary of MCP targeting abilities for alanine substitutions in PduP$^{1-18}$**
Fluorescence microscopy was used to assess GFP targeting to microcompartments via variants of the PduP$^{1-18}$ signal sequence. The appearance of punctate fluorescence within cells is considered successful (+), and the lack of such puncta is considered unsuccessful (-), while mutants that confer faint punctate fluorescence with high cellular background represent very low levels of encapsulation (-*).

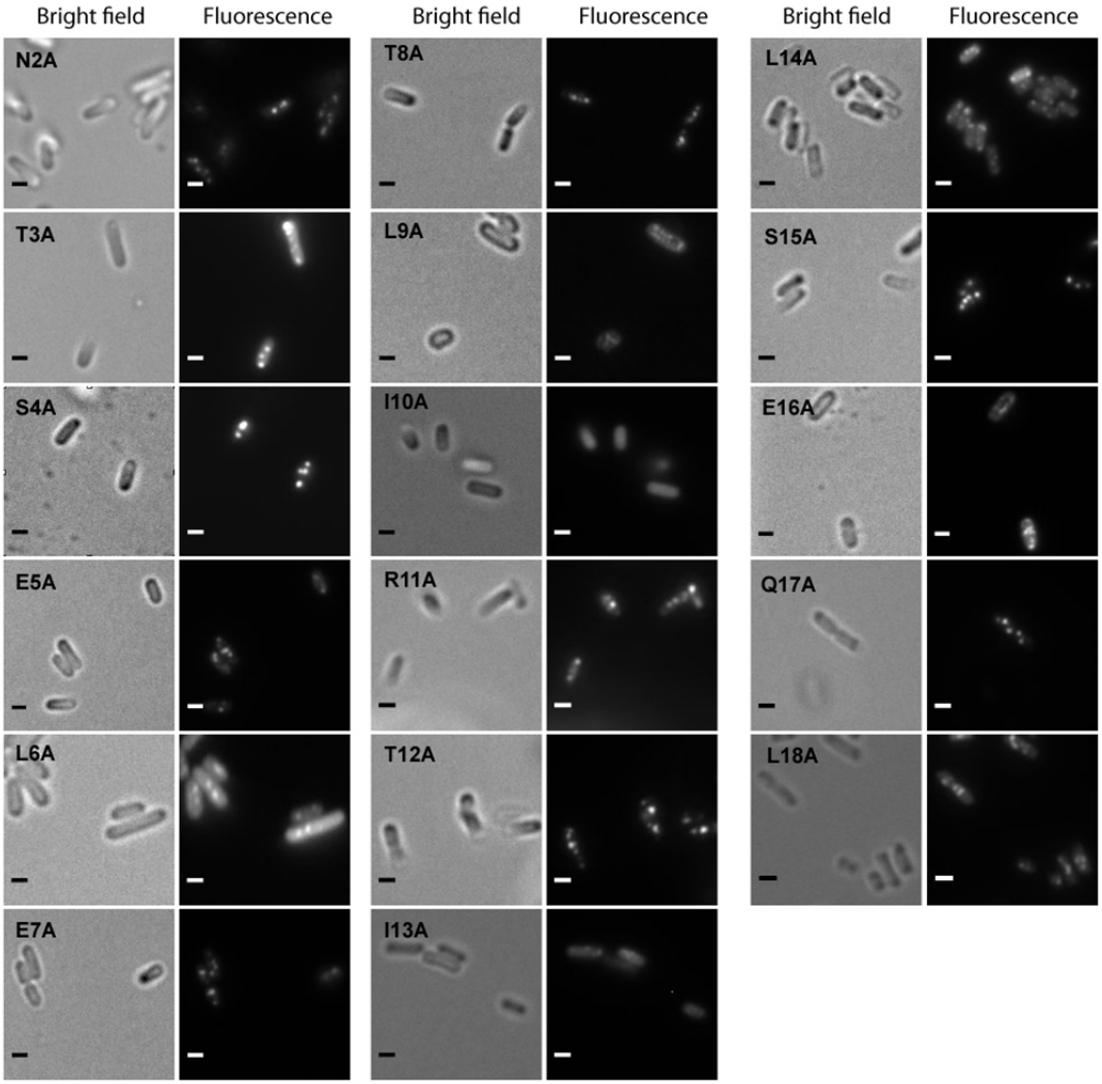


**Figure 4.8: MCP targeting abilities for alanine substitutions in PduP$^{1-18}$ by fluorescence microscopy**

Fluorescence microscopy is used to assess targeting of a GFP reporter fusion protein via an alanine scan library of the PduP$^{1-18}$ signal sequence. Cells expressing successfully encapsulated reporter protein display punctate fluorescence, whereas cells expressing encapsulation-impaired reporter protein display diffuse fluorescence.

The PduP$^{1-18}$ alanine mutants were next fused with GFP–SsrA, and flow cytometry data was collected for cells expressing the resulting library. Some mutations (T3A, S4A, R11A, and T12A) result in a higher level of protein encapsulation than wild type as measured by total cellular fluorescence, with T3A conferring a fluorescence ratio greater than twice that of wild type (Figure 4.9). A western blot of purified MCPs from selected mutants corroborates the flow cytometry findings (T3A>S4A>wild type signal sequence as measured by GFP band intensities, Figure 4.10).

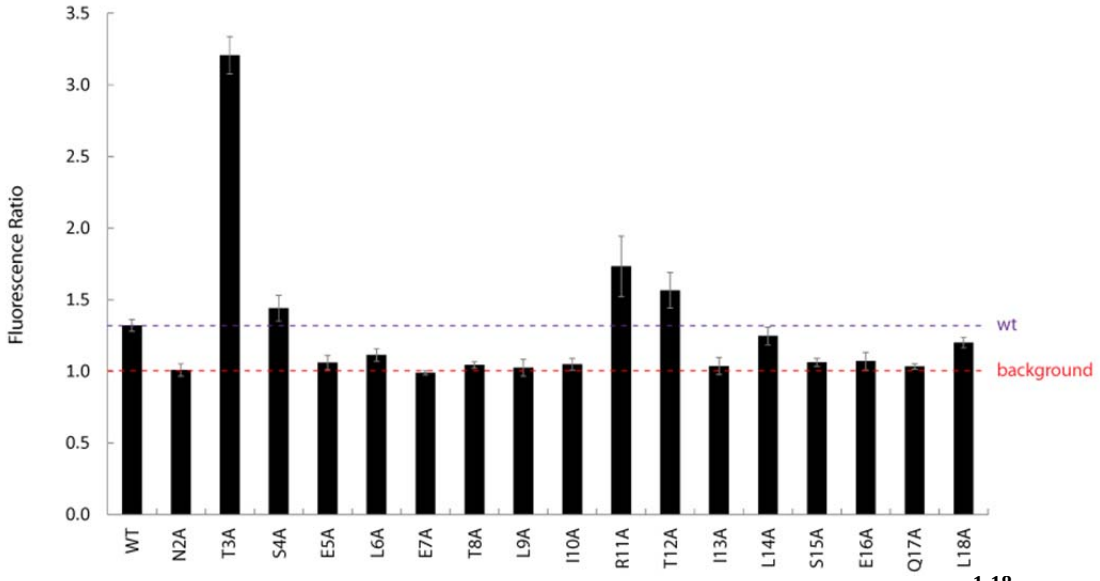


**Figure 4.9: Flow cytometry fluorescence ratios of an alanine scan of the PduP$^{1-18}$ –GFP-SsrA**

Ratios are given as the average fluorescence for cells grown in 1,2-PD over the average fluorescence for cells grown in the absence of 1,2-PD.

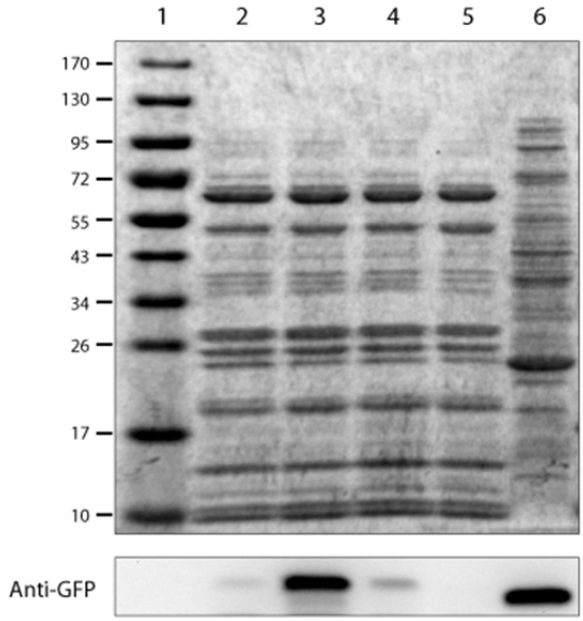


**Figure 4.10: Anti-GFP western blot shows differential encapsulation amounts of GFP for different signal sequence mutants**

4%-20% SDS-PAGE gel and anti-GFP western blot of a (lane 1) molecular mass marker, and purified MCPs from *S. enterica* expressing (lane 2) PduP$^{1-18}$-GFP-SsrA, (lane 3) PduP$^{1-18}$T3A-GFP-SsrA, (lane 4) PduP$^{1-18}$S4A-GFP-SsrA, and (lane 5) GFP-SsrA, along with cell lysate from *S. enterica* expressing PduP$^{1-18}$-GFP (Lane 6). Lanes with purified MCPs were loaded with 5 μg of total protein.

Surprisingly, we found that many mutations that were permissive for MCP encapsulation in the PduP$^{1-18}$-GFP alanine scan library via fluorescence microscopy have a fluorescence ratio close to one in the PduP$^{1-18mut}$-GFP-SsrA flow cytometry assay. We believe this is due to the added stringency from adding the SsrA degradation tag, which now requires that the signal sequence-tagged GFP must be encapsulated faster than it can be degraded by the ClpXP protease. This may be a serendipitous advantage for screening for optimal signal sequences; as one purpose of compartmentalizing enzymes into MCPs may be to mitigate the effects of toxic intermediates, the rapid clearance of unencapsulated enzymes will minimize the cytosolic formation of these compounds.

### *4.3.4 Truncations and minimal requirements for targeting*

Previous work to identify the Pdu MCP targeting sequence investigated the first 10,14, 18, and 70 amino acids of PduP [18]. When fused to GFP, the amount of GFP detected by western blotting in purified MCPs increased with increasing length of the N-terminal PduP signal sequence. Here, we have used the newly developed flow cytometry assay to more systematically investigate the encapsulation strength of PduP$^{1-18}$ truncations.

The results show a decreasing amount of encapsulation, as detected by fluorescence, for C-terminal truncations from PduP$^{1-18}$ to PduP$^{1-16}$, and minimal fluorescence for further C-terminal truncations (Figure 4.11). For N-terminal truncations, the initial methionine was kept in the first amino acid position. Elimination of the first amino acid after methionine (PduP$^{3-18}$) results in low fluorescence. However, a high fluorescence level is observed for PduP$^{4-18}$. Interestingly, this truncation eliminated Thr3, which when mutated to alanine in our previous experiment, also conferred high fluorescence. Further N-terminal truncations once again result in low fluorescence. We also examined the effect of combining N-terminal and C-terminal truncations; PduP$^{3-17}$ and PduP$^{3-16}$ confer low fluorescence, while PduP$^{4-17}$ gives rise to higher fluorescence than wild type, but still less than PduP$^{4-18}$. These results provide additional clues about the role of each amino acid of the PduP signal sequence.

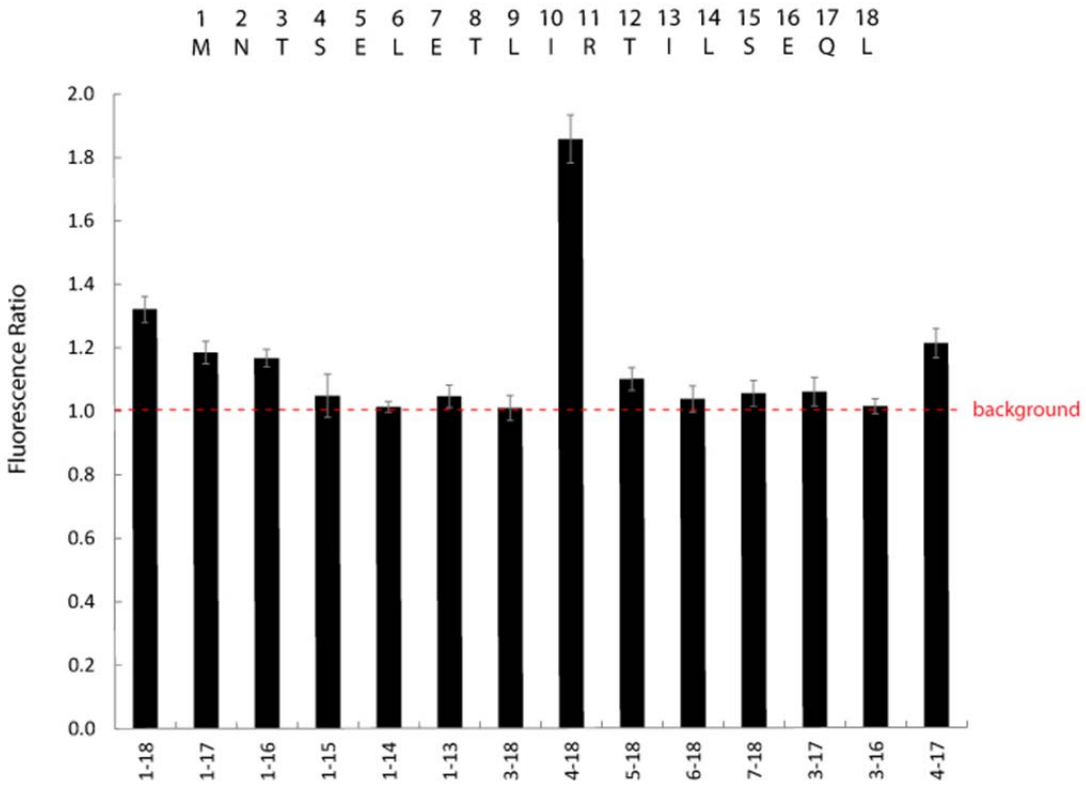


**Figure 4.11: Flow cytometry fluorescence ratio of a various truncations of the PduP signal sequence**
Ratios are given as the average fluorescence for cells grown in 1,2-PD over the average fluorescence for cells grown in the absence of 1,2-PD. The samples are named by the beginning and ending amino acid position of the wild type PduP sequence of *S. enterica* serovar Typhimurium LT2.

### *4.3.5 Single amino acid substitution library*

A major advantage of this assay is that it can be performed with higher throughput and in an automated process as compared to microscopy or western blotting of purified MCPs. We have applied this assay to screen a library of single amino acid substitution mutants in key positions in the signal sequence. For each amino acid position studied, a mutant library was constructed using NNK primers and placed in a pBAD33 expression vector to create $PduP^{1\text{-}18mut}$-GFP-SsrA. The NNK codon can encode for any of the twenty naturally occurring amino acids. From each library, 96 colonies were sequenced and data was collected using flow cytometry.

The results are shown as a heat map (Figure 4.12). The data show that several amino acid positions in $PduP^{1\text{-}18}$ are highly intolerant to mutations. These include the hydrophobic residues Leu9, Ile10, and Ile13, which is consistent with what we observed from the previous alanine scan. In addition, the negatively charged residues Glu5, Glu7, and Glu16 are also highly intolerant to mutations. One discrepancy of note is that Glu7Glu has a low fluorescence ratio.

However, all mutants tested for Glu7Glu were of a less frequent codon (GAG) than wild type (GAA) due to the nature of using NNK primers in the construction of the mutant library. Therefore, it is likely that this observation is due to decreased expression levels. Due to the nature of this assay, a negative result due to low expression cannot be distinguished from non-compartmentalization.

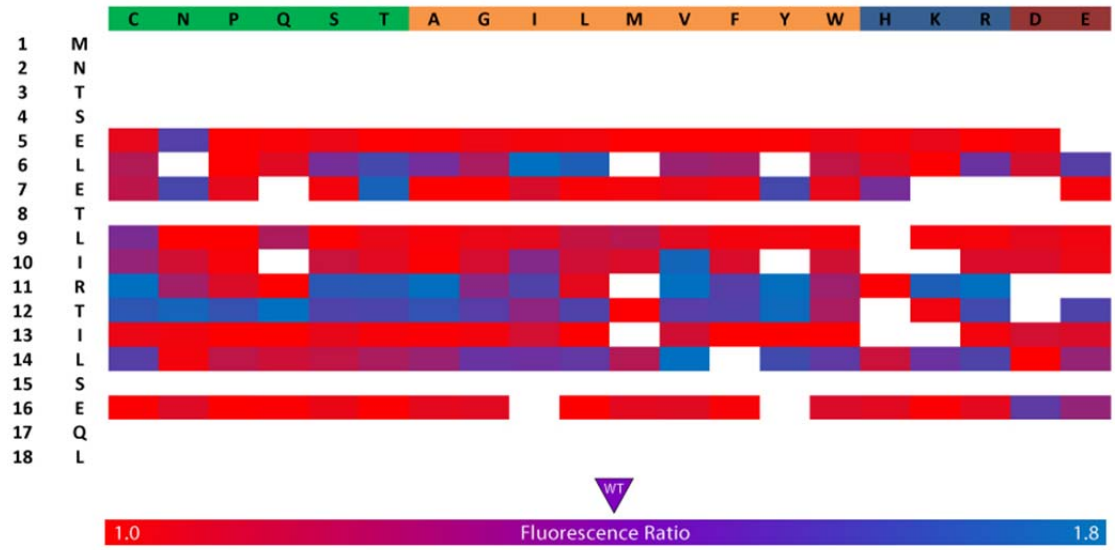


**Figure 4.12: Heat map of flow cytometry fluorescence ratios for single amino acid substitutions for various positions in the PduP$^{1-18}$ signal sequence**
For each amino acid position, 96 mutant strains were selected. The left side lists the position and original amino acid sequence for PduP$^{1-18}$. The top lists the amino acid residue to which the position was mutated, grouped by amino acid characteristic: green for polar residues, orange for hydrophobic residues, blue for positively charged residues, and red for negatively charged residues. Within the heat map are the results from the flow cytometry assay: relative to the wild type sequence, red indicates a low fluorescence ratio, blue represents a high fluorescence ratio, and white represents mutants that were not found or tested within the library.

Several of the mutants in this study were found to have greater protein encapsulation than WT. Many of these were found in mutations to Arg 11 and Thr 12. These mutated signal sequences may be of interest to encapsulate increased amounts of enzyme into MCPs to maximize flux of encapsulated synthetic pathways. In addition to finding signal sequences for maximized protein encapsulation, these results provide insight into the rules for encapsulation using the PduP$^{1-18}$ signal sequence.

## 4.4 Discussion and Future Directions

Prior to this study, detection of protein encapsulation in MCPs was limited to low throughput methods such as fluorescence microscopy and western blotting of purified MCPs. In an effort to further characterize the MCP targeting signal sequence we developed a flow cytometry assay for the rapid detection of the encapsulation of fluorescent reporter proteins. This method is performed *in vivo* and therefore bypasses the lengthy process of purifying MCPs. Furthermore, flow cytometry can be automated in a 96 well plate format. In addition to enabling higher throughput analysis, this flow cytometry assay allows for measuring the range of protein encapsulation in a more quantitative manner than previous methods. It is important to note, however, that protein encapsulation is in equilibrium with protein production and degradation; this assay does not decouple these individual contributions, but instead reports the net sum of these factors.

We have used this assay to characterize the level of protein encapsulation for various mutations in the $PduP^{1-18}$ signal sequence. Some of these mutants confer enhanced protein encapsulation as compared to the wild-type signal sequence, which may be useful for maximizing titer in encapsulated synthetic pathways. In addition, a library of signal sequences with varying encapsulation signal strengths may permit control over enzyme stoichiometry when compartmentalizing multiple-enzyme pathways; stoichiometry has been shown to have a large impact on product titer for a scaffolded mevalonate synthesis pathway[2].

This flow cytometry assay lends itself to a number of applications. For instance, the assay could be applied to identify the yet-undetermined signal sequence for encapsulation in carboxysomes. It could also be used to study the effects of competition among different signal sequences, or to eliminate encapsulation competition by creating orthogonal shell-signal sequence binding pairs for increased control over encapsulated pathways. The assay also enables future investigations into the impact of binding kinetics on encapsulation. We have shown that this flow cytometry assay is a powerful tool for the investigation of protein encapsulation and the development of MCP-based nanobioreactors.

# Chapter 5: CONCLUSIONS

At the start of this work, bacterial MCPs were a new and largely unexplored field. In this work we present our efforts toward understanding the Pdu MCP system and developing it into an engineerable tool.

In Chapter 2, we describe our characterization of Pdu MCP stability over time, at elevated temperatures, and in buffers of various pH and salt concentration. We find that MCPs are robust to temperatures up to 60°C and are stable for weeks when stored at 4°C. While the Pdu MCP is susceptible to non-physiological pH and salt concentrations, this may prove to be a useful in such applications as endosomal escape during drug delivery. This study demonstrates that MCPs have the stability required for many of their proposed applications.

We then explore the regulation of the Pdu MCP. In Chapter 3 we find that growth in the rich media LB does not inhibit MCP formation or encapsulation of proteins within. We then show the first instance of Pdu MCP formation in a heterologous organism, *E. coli*, in which TEM images show MCPs of similar size and shape as MCPs from the native host *S. enterica*. These two findings will make the Pdu MCP more accessible for future studies and applications.

Finally, in Chapter 4 we investigate the rules for encapsulating proteins within the Pdu MCP. We start by developing a high throughput assay for detecting encapsulation of a fluorescence reporter. We then use this assay in a number of studies to find a motif of hydrophobic and charged residues in the localization signal sequence. From this study we have generated a library of signal sequence mutants with different targeting strengths which can be used to control the amount of protein loaded into MCPs or control enzyme stoichiometry in encapsulated multi-enzyme pathways.

Taken together, this work expands our knowledge of the Pdu MCP and demonstrates that key elements of the system can be engineered.

# REFERENCES


1. Moon TS, Dueber JE, Shiue E, & Prather KLJ (2010) Use of modular, synthetic scaffolds for improved production of glucaric acid in engineered E. coli. *Metab. Eng.* 12(3):298-305.
2. Dueber JE, *et al.* (2009) Synthetic protein scaffolds provide modular control over metabolic flux. *Nat. Biotechnol.* 27(8):753-759.
3. Conrado RJ, *et al.* (2012) DNA-guided assembly of biosynthetic pathways promotes improved catalytic efficiency. *Nucleic Acids Res.* 40(4):1879-1889.
4. Conrado RJ, Mansell TJ, Varner JD, & DeLisa MP (2007) Stochastic reaction-diffusion simulation of enzyme compartmentalization reveals improved catalytic efficiency for a synthetic metabolic pathway. *Metab. Eng.* 9(4):355-363.
5. Vriezema DM, *et al.* (2005) Self-assembled nanoreactors. *Chemical Reviews* 105(4):1445-1489.
6. Glasgow JE, Capehart SL, Francis MB, & Tullman-Ercek D (2012) Osmolyte-Mediated Encapsulation of Proteins inside MS2 Viral Capsids. *ACS Nano* 6(10):8658-8664.
7. Fiedler JD, Brown SD, Lau JL, & Finn MG (2010) RNA-directed packaging of enzymes within virus-like particles. *Angew Chem Int Ed Engl* 49(50):9648-9651.
8. Minten IJ, Nolte RJM, & Cornelissen JJLM (2010) Complex Assembly Behavior During the Encapsulation of Green Fluorescent Protein Analogs in Virus Derived Protein Capsules. *Macromol. Biosci.* 10(5):539-545.
9. O'Neil A, Reichhardt C, Johnson B, Prevelige PE, & Douglas T (2011) Genetically Programmed In Vivo Packaging of Protein Cargo and Its Controlled Release from Bacteriophage P22. *Angewandte Chemie-International Edition* 50(32):7425-7428.
10. Ashley CE, *et al.* (2011) Cell-specific delivery of diverse cargos by bacteriophage MS2 virus-like particles. *ACS Nano* 5(7):5729-5745.
11. Rhee JK, *et al.* (2011) Colorful virus-like particles: fluorescent protein packaging by the Qbeta capsid. *Biomacromolecules* 12(11):3977-3981.
12. Worsdorfer B, Pianowski Z, & Hilvert D (2012) Efficient in vitro encapsulation of protein cargo by an engineered protein container. *J. Am. Chem. Soc.* 134(2):909-911.
13. Worsdorfer B, Woycechowsky KJ, & Hilvert D (2011) Directed evolution of a protein container. *Science* 331(6017):589-592.
14. Quellec P, *et al.* (1999) Protein encapsulation within poly(ethylene glycol)-coated nanospheres. II. Controlled release properties. *J Biomed Mater Res* 47(3):388-395.
15. Quellec P, *et al.* (1998) Protein encapsulation within polyethylene glycol-coated nanospheres. I. Physicochemical characterization. *J Biomed Mater Res* 42(1):45-54.
16. Colletier JP, Chaize B, Winterhalter M, & Fournier D (2002) Protein encapsulation in liposomes: efficiency depends on interactions between protein and phospholipid bilayer. *BMC Biotechnol.* 2:9.
17. Sutter M, *et al.* (2008) Structural basis of enzyme encapsulation into a bacterial nanocompartment. *Nat. Struct. Mol. Biol.* 15(9):939-947.
18. Fan C, *et al.* (2010) Short N-terminal sequences package proteins into bacterial microcompartments. *Proc Natl Acad Sci U S A* 107(16):7509-7514.
19. Drews G & Niklowitz W (1956) [Cytology of Cyanophycea. II. Centroplasm and granular inclusions of Phormidium uncinatum]. *Arch Mikrobiol* 24(2):147-162.
20. Yeates TO, Crowley CS, & Tanaka S (2010) Bacterial microcompartment organelles: protein shell structure and evolution. *Annu Rev Biophys* 39:185-205.
21. Crowley CS, Sawaya MR, Bobik TA, & Yeates TO (2008) Structure of the PduU shell protein from the Pdu microcompartment of Salmonella. *Structure* 16(9):1324-1332.

22. Crowley CS, *et al.* (2010) Structural insight into the mechanisms of transport across the Salmonella enterica Pdu microcompartment shell. *J. Biol. Chem.* 285(48):37838-37846.
23. Pang A, Warren MJ, & Pickersgill RW (2011) Structure of PduT, a trimeric bacterial microcompartment protein with a 4Fe-4S cluster-binding site. *Acta Crystallogr D Biol Crystallogr* 67(Pt 2):91-96.
24. Sagermann M, Ohtaki A, & Nikolakakis K (2009) Crystal structure of the EutL shell protein of the ethanolamine ammonia lyase microcompartment. *Proc Natl Acad Sci U S A* 106(22):8883-8887.
25. Tanaka S, Sawaya MR, & Yeates TO (2010) Structure and mechanisms of a protein-based organelle in Escherichia coli. *Science* 327(5961):81-84.
26. Kerfeld CA, *et al.* (2005) Protein structures forming the shell of primitive bacterial organelles. *Science* 309(5736):936-938.
27. Tanaka S, *et al.* (2008) Atomic-level models of the bacterial carboxysome shell. *Science* 319(5866):1083-1086.
28. Tsai Y, *et al.* (2007) Structural analysis of CsoS1A and the protein shell of the Halothiobacillus neapolitanus carboxysome. *PLoS Biol.* 5(6):e144.
29. Tsai Y, Sawaya MR, & Yeates TO (2009) Analysis of lattice-translocation disorder in the layered hexagonal structure of carboxysome shell protein CsoS1C. *Acta Crystallogr D Biol Crystallogr* 65(Pt 9):980-988.
30. Klein MG, *et al.* (2009) Identification and structural analysis of a novel carboxysome shell protein with implications for metabolite transport. *J. Mol. Biol.* 392(2):319-333.
31. Wheatley NM, Gidaniyan SD, Liu Y, Cascio D, & Yeates TO (2013) Bacterial microcompartment shells of diverse functional types possess pentameric vertex proteins. *Protein Sci.* 22(5):660-665.
32. Kerfeld CA, Heinhorst S, & Cannon GC (2010) Bacterial microcompartments. *Annu. Rev. Microbiol.* 64:391-408.
33. Takenoya M, Nikolakakis K, & Sagermann M (2010) Crystallographic insights into the pore structures and mechanisms of the EutL and EutM shell proteins of the ethanolamine-utilizing microcompartment of Escherichia coli. *J. Bacteriol.* 192(22):6056-6063.
34. Parsons JB, *et al.* (2008) Biochemical and structural insights into bacterial organelle form and biogenesis. *J. Biol. Chem.* 283(21):14366-14375.
35. Parsons JB, *et al.* (2010) Synthesis of Empty Bacterial Microcompartments, Directed Organelle Protein Incorporation, and Evidence of Filament-Associated Organelle Movement. *Mol. Cell* 38(2):305-315.
36. Sinha S, Cheng S, Fan C, & Bobik TA (2012) The PduM protein is a structural component of the microcompartments involved in coenzyme B(12)-dependent 1,2-propanediol degradation by Salmonella enterica. *J. Bacteriol.* 194(8):1912-1918.
37. Cheng S, Sinha S, Fan C, Liu Y, & Bobik TA (2011) Genetic analysis of the protein shell of the microcompartments involved in coenzyme B12-dependent 1,2-propanediol degradation by Salmonella. *J. Bacteriol.* 193(6):1385-1392.
38. Choudhary S, Quin MB, Sanders MA, Johnson ET, & Schmidt-Dannert C (2012) Engineered protein nano-compartments for targeted enzyme localization. *PLoS One* 7(3):e33342.
39. Bonacci W, *et al.* (2012) Modularity of a carbon-fixing protein organelle. *Proc Natl Acad Sci U S A* 109(2):478-483.
40. Fan C & Bobik TA (2011) The N-terminal region of the medium subunit (PduD) packages adenosylcobalamin-dependent diol dehydratase (PduCDE) into the Pdu microcompartment. *J. Bacteriol.* 193(20):5623-5628.
41. Kinney JN, Salmeen A, Cai F, & Kerfeld CA (2012) Elucidating essential role of conserved carboxysomal protein CcmN reveals common feature of bacterial microcompartment assembly. *J. Biol. Chem.* 287(21):17729-17736.

42. Fan C, Cheng S, Sinha S, & Bobik TA (2012) Interactions between the termini of lumen enzymes and shell proteins mediate enzyme encapsulation into bacterial microcompartments. *Proc Natl Acad Sci U S A* 109(37):14995-15000.
43. Bobik TA, Havemann GD, Busch RJ, Williams DS, & Aldrich HC (1999) The propanediol utilization (pdu) operon of Salmonella enterica serovar Typhimurium LT2 includes genes necessary for formation of polyhedral organelles involved in coenzyme B(12)-dependent 1, 2-propanediol degradation. *J. Bacteriol.* 181(19):5967-5975.
44. Havemann GD, Sampson EM, & Bobik TA (2002) PduA is a shell protein of polyhedral organelles involved in coenzyme B(12)-dependent degradation of 1,2-propanediol in Salmonella enterica serovar typhimurium LT2. *J. Bacteriol.* 184(5):1253-1261.
45. Sampson EM & Bobik TA (2008) Microcompartments for B12-dependent 1,2-propanediol degradation provide protection from DNA and cellular damage by a reactive metabolic intermediate. *J. Bacteriol.* 190(8):2966-2971.
46. Yeates TO, Kerfeld CA, Heinhorst S, Cannon GC, & Shively JM (2008) Protein-based organelles in bacteria: carboxysomes and related microcompartments. *Nat. Rev. Microbiol.* 6(9):681-691.
47. Cheng S, Liu Y, Crowley CS, Yeates TO, & Bobik TA (2008) Bacterial microcompartments: their properties and paradoxes. *Bioessays* 30(11-12):1084-1095.
48. Kim EY & Tullman-Ercek D (2013) Engineering nanoscale protein compartments for synthetic organelles. *Curr. Opin. Biotechnol.* 24(4):627-632.
49. Kovacs EW*, et al.* (2007) Dual-surface-modified bacteriophage MS2 as an ideal scaffold for a viral capsid-based drug delivery system. *Bioconjug Chem* 18(4):1140-1147.
50. Ma Y, Nolte RJ, & Cornelissen JJ (2012) Virus-based nanocarriers for drug delivery. *Adv Drug Deliv Rev* 64(9):811-825.
51. Kwak M*, et al.* (2010) Virus-like particles templated by DNA micelles: a general method for loading virus nanocarriers. *J. Am. Chem. Soc.* 132(23):7834-7835.
52. Stonehouse NJ & Stockley PG (1993) Effects of amino acid substitution on the thermal stability of MS2 capsids lacking genomic RNA. *FEBS Lett.* 334(3):355-359.
53. Anonymous (!!! INVALID CITATION !!!).
54. Feng YY, Ong SL, Hu JY, Tan XL, & Ng WJ (2003) Effects of pH and temperature on the survival of coliphages MS2 and Qbeta. *J. Ind. Microbiol. Biotechnol.* 30(9):549-552.
55. Lavelle L, Michel JP, & Gingery M (2007) The disassembly, reassembly and stability of CCMV protein capsids. *J. Virol. Methods* 146(1-2):311-316.
56. Bancroft JB, McDonald JG, & Rees MW (1976) A mutant of cowpea chlorotic mottle virus with a perturbed assembly mechanism. *Virology* 75(2):293-305.
57. Vogel HJ & Bonner DM (1956) Acetylornithinase of Escherichia coli: partial purification and some properties. *J. Biol. Chem.* 218(1):97-106.
58. Lavinder JJ, Hari SB, Sullivan BJ, & Magliery TJ (2009) High-throughput thermal scanning: a general, rapid dye-binding thermal shift screen for protein engineering. *J. Am. Chem. Soc.* 131(11):3794-3795.
59. Phillips K & de la Pena AH (2011) The combined use of the Thermofluor assay and ThermoQ analytical software for the determination of protein stability and buffer optimization as an aid in protein crystallization. *Curr Protoc Mol Biol* Chapter 10:Unit10 28.
60. Ericsson UB, Hallberg BM, Detitta GT, Dekker N, & Nordlund P (2006) Thermofluor-based high-throughput stability optimization of proteins for structural studies. *Anal. Biochem.* 357(2):289-298.
61. Havemann GD & Bobik TA (2003) Protein content of polyhedral organelles involved in coenzyme B12-dependent degradation of 1,2-propanediol in Salmonella enterica serovar Typhimurium LT2. *J. Bacteriol.* 185(17):5086-5095.
62. Rybak SL & Murphy RF (1998) Primary cell cultures from murine kidney and heart differ in endosomal pH. *J Cell Physiol* 176(1):216-222.

63. Sipe DM, Jesurum A, & Murphy RF (1991) Absence of Na+,K(+)-ATPase regulation of endosomal acidification in K562 erythroleukemia cells. Analysis via inhibition of transferrin recycling by low temperatures. *J. Biol. Chem.* 266(6):3469-3474.
64. Killisch I*, et al.* (1992) Characterization of early and late endocytic compartments of the transferrin cycle. Transferrin receptor antibody blocks erythroid differentiation by trapping the receptor in the early endosome. *J. Cell Sci.* 103 ( Pt 1):211-232.
65. Savage DF, Afonso B, Chen AH, & Silver PA (2010) Spatially ordered dynamics of the bacterial carbon fixation machinery. *Science* 327(5970):1258-1261.
66. Rondon MR & Escalante-Semerena JC (1992) The poc locus is required for 1,2-propanediol-dependent transcription of the cobalamin biosynthetic (cob) and propanediol utilization (pdu) genes of Salmonella typhimurium. *J. Bacteriol.* 174(7):2267-2272.
67. Walter D, Ailion M, & Roth J (1997) Genetic characterization of the pdu operon: use of 1,2-propanediol in Salmonella typhimurium. *J. Bacteriol.* 179(4):1013-1022.
68. Chen P, Ailion M, Bobik T, Stormo G, & Roth J (1995) Five promoters integrate control of the cob/pdu regulon in Salmonella typhimurium. *J. Bacteriol.* 177(19):5401-5410.
69. Ailion M, Bobik TA, & Roth JR (1993) Two global regulatory systems (Crp and Arc) control the cobalamin/propanediol regulon of Salmonella typhimurium. *J. Bacteriol.* 175(22):7200-7208.
70. Sargent F*, et al.* (2013) A synthetic system for expression of components of a bacterial microcompartment. *Microbiology* 159(Pt 11):2427-2436.
71. Katoh K, Misawa K, Kuma K, & Miyata T (2002) MAFFT: a novel method for rapid multiple sequence alignment based on fast Fourier transform. *Nucleic Acids Res.* 30(14):3059-3066.
72. Farrell CM, Grossman AD, & Sauer RT (2005) Cytoplasmic degradation of ssrA-tagged proteins. *Mol. Microbiol.* 57(6):1750-1761.
73. Gottesman S, Roche E, Zhou Y, & Sauer RT (1998) The ClpXP and ClpAP proteases degrade proteins with carboxy-terminal peptide tails added by the SsrA-tagging system. *Genes Dev.* 12(9):1338-1347.
74. Karzai AW, Roche ED, & Sauer RT (2000) The SsrA-SmpB system for protein tagging, directed degradation and ribosome rescue. *Nat. Struct. Biol.* 7(6):449-455.
75. DeLisa MP, Samuelson P, Palmer T, & Georgiou G (2002) Genetic analysis of the twin arginine translocator secretion pathway in bacteria. *J. Biol. Chem.* 277(33):29825-29831.